

NACA RM E9H15

11153  
205  
6

~~CONFIDENTIAL~~  
**NACA**

# RESEARCH MEMORANDUM

DOWNWASH IN VORTEX REGION BEHIND TRAPEZOIDAL-WING  
TIP AT MACH NUMBER 1.91

By J. L. Cummings, H. Mirels, and L. E. Baughman

Lewis Flight Propulsion Laboratory  
Cleveland, Ohio

CLASSIFICATION CANCELLED

CLASSIFIED DOCUMENT

Authority NACA R 72456 Date 2/18/54  
By DATA 9/8/54 See \_\_\_\_\_

This document contains classified information affecting the National Defense of the United States within the meaning of the Espionage Act, USC 50-31 and 32. Its transmission or the revelation of its contents in any manner to an unauthorized person is prohibited by law. Information so classified may be imparted only to persons in the military and naval services of the United States, appropriate civilian officers and employees of the Federal Government who have a legitimate interest therein, and to United States citizens of known loyalty and discretion who of necessity must be informed thereof.

## NATIONAL ADVISORY COMMITTEE FOR AERONAUTICS

WASHINGTON  
November 10, 1949

UNCLASSIFIED



UNCLASSIFIED

## NATIONAL ADVISORY COMMITTEE FOR AERONAUTICS

RESEARCH MEMORANDUM

DOWNWASH IN VORTEX REGION BEHIND TRAPEZOIDAL-WING

TIP AT MACH NUMBER 1.91

By J. L. Cummings, H. Mirels, and L. E. Baughman

## SUMMARY

The results of an experimental investigation to determine the downwash in the region of the trailing vortex system behind a trapezoidal-wing tip in a supersonic stream are presented. The wing was cut along the inner Mach line from the tip and had a 5-percent-thick symmetrical diamond cross section. The investigation was made at a Mach number of 1.91 and a Reynolds number of  $1.56 \times 10^6$  based on the wing chord. A wake survey was also conducted.

For small angles of attack, the experimental spanwise variation of  $-d\epsilon/d\alpha$  (where  $\epsilon$  is the downwash angle and  $\alpha$  is the angle of attack) at each chordwise station was generally similar to the variation predicted by linearized theory. At higher angles of attack, the spanwise location of the maximum value of  $-d\epsilon/d\alpha$  at each chordwise station occurred nearer the center of the theoretical vortex sheet than linearized theory would indicate. This result was mainly attributed to differences between the theoretical and actual spanwise distribution of vorticity and to the distortion of the vortex sheet, but the individual effects could not be isolated. A survey of the friction wake indicated several characteristics similar to those observed in subsonic flow.

## INTRODUCTION

A knowledge of the downwash behind supersonic lifting surfaces is necessary for the rational design of supersonic airplane or missile configurations. Methods for obtaining linearized solutions for the downwash behind supersonic wings are now available (for example, references 1 to 3). Linearized theory, however, assumes thin wings at small angles of attack and neglects viscous effects and the displacement and the distortion of the trailing vortex system. An experimental program is required to check the indications of linearized theory and to determine the necessary

UNCLASSIFIED

modifications that will result in agreement between theory and experiment. A comprehensive program of this type for subsonic wings is presented in reference 4.

An investigation of the downwash behind a rectangular wing at a Mach number of 1.53 is reported in reference 5. Experimental trends of the variation of downwash angle with angle of attack at zero lift were similar to those predicted by linearized theory. The comparison between theory and experiment also indicated that the displacement of the vortex sheet and the resulting influence on the downwash distribution should be considered in calculating downwash angles at finite angles of attack. These results are analogous to those presented in reference 4 for the subsonic case and illustrate the interdependence of the downwash and the trailing vortex system.

An investigation was undertaken at the NACA Lewis laboratory to obtain downwash data in the immediate vicinity of the trailing vortex sheet, rather than in a probable tail-surface location, in order to provide data relating the shed vorticity and the downwash behind supersonic wings. The results for a trapezoidal wing are presented.

#### SYMBOLS

The following symbols are used in this report:

$C_{p,B}$  pressure coefficient, bottom surface of wing

$C_{p,T}$  pressure coefficient, top surface of wing

$c$  wing chord (0.5 ft on model)

$H$  pitot pressure in free stream

$H_w$  pitot pressure in wake

$\Delta H$   $H - H_w$

$M$  Mach number

$m$  slope of inclined vortex sheet (fig. 6)

$$R = \frac{x - \sqrt{x^2 - \beta^2(y^2 + z^2)}}{\beta \sqrt{y^2 + z^2}}$$

$$R' = \frac{\frac{x}{c} - 1 - \sqrt{\left(\frac{x}{c} - 1\right)^2 - \left[\left(\frac{\beta y}{c} + 1\right)^2 + \left(\frac{\beta z}{c}\right)^2\right]}}{\sqrt{\left(\frac{\beta y}{c} + 1\right)^2 + \left(\frac{\beta z}{c}\right)^2}}$$

$$T = \frac{x - \sqrt{x^2 - (\beta y)^2}}{\beta y}$$

$$T' = \frac{\frac{x}{c} - 1 - \sqrt{\left(\frac{x}{c} - 1\right)^2 - \left(\frac{\beta y}{c} + 1\right)^2}}{\frac{\beta y}{c} + 1}$$

t thickness of vortex system (fig. 8)

U free-stream velocity

$\left. \begin{array}{l} x \\ y \\ z \end{array} \right\}$  Cartesian coordinate system with origin at tip  
of leading edge of wing at  $0^\circ$  angle of attack,  
(fig. 4)

$\alpha$  angle of attack

$$\beta = \sqrt{M^2 - 1}$$

$\Gamma$  circulation of wing

$\epsilon$  downwash angle (positive in negative z-direction)

$$\theta = \arctan \frac{z}{y}$$

$$\theta' = \arctan' \frac{\frac{\beta z}{c}}{\frac{\beta y}{c} + 1}$$

Subscripts:

l leading edge

t trailing edge

o variable of integration

## APPARATUS

The investigation was conducted in the NACA Lewis 18- by 18-inch supersonic wind tunnel. From tunnel calibration, the Mach number in the region of the wing and in the region surveyed was found to be  $1.91 \pm 0.01$ . The stagnation temperature of the air was held at approximately  $150^{\circ}$  F and the dew point at  $-10^{\circ}$  F. The Reynolds number based on the wing chord was  $1.56 \times 10^6$ .

The model investigated was a trapezoidal half-wing with the side edge cut along the inner Mach line (fig. 1). The wing was machined from SAE 4140 steel and had finished surfaces ground to 16 microinches and knife edges at the leading and trailing edges. The wing was mounted on the tunnel wall (fig. 1) and could be pivoted about the midpoint of the root chord. The angle of attack was read to an accuracy of  $\pm 0.05^{\circ}$ .

The angle of downwash was determined with a symmetrical wedge (fig. 2) that could be rotated about its leading edge. The wedge had a  $15^{\circ}$  half-angle with a static orifice on and a pitot-pressure (local total pressure behind normal shock wave) tube above each face. A flexible cable from outside the tunnel turned a worm and a worm-gear-segment combination that rotated the wedge. The angular position of the wedge was indicated by a revolution counter coupled to the worm shaft. The wedge angle of attack could be read to an accuracy of  $\pm 0.10^{\circ}$ . The static-pressure differential of the wedge was read on a U-tube water manometer.

The wedge mechanism was mounted on a support that could be moved to any position behind the wing in the free-stream x- and cross-tunnel z-directions. The support could be moved spanwise (y coordinate) in  $7/8$ -inch steps. The wedge could be set with an accuracy of  $\pm 0.015$  inch in the z-direction and  $\pm 0.025$  inch in the y-direction before starting the tunnel. A cathetometer was used to set the position of the wedge in the x-direction to an accuracy of  $\pm 0.0039$  inch while the tunnel was in operation.

The wake was surveyed with a pitot-pressure rake of 41 tubes with a 0.015-inch outside diameter and spaced 0.05 inch apart (fig. 3(a)). The tubes were alternately spaced in each of two rows 0.08 inch apart. The rake was mounted normal to the undisturbed free stream on the same support that was used for the wedge mechanism (fig. 3(b)). Pressures were read on a differential tetrabromoethane multiple-tube manometer board.

## PROCEDURE

The angle of downwash was determined by the null method, which consists in adjusting the angle of attack of the wedge until the static pressure on the two wedge faces are equal. When the two static pressures are balanced, the wedge angle of attack is recorded. The angle of downwash was taken to be the difference between the wedge angle of attack with the wing at zero angle of attack and at the actual angle of attack. The downwash was measured in the  $z = 0$  plane over a range of angle of attack from  $8^\circ$  to  $-8^\circ$  at each of the stations shown in figure 4. Chordwise stations are designated by their distance in inches behind the leading edge of the wing. The static-pressure orifice and the pitot-pressure tube of the wedge (fig. 2) permit calculation of the local Mach number at each station.

The wake survey was made behind the wing at angles of attack of  $0^\circ$ ,  $\pm 4^\circ$ , and  $\pm 8^\circ$ . The pitot pressures were measured by the survey rake to determine the wake displacement and the thickness.

## THEORY

Linearized theory yields closed-form expressions (reference 1) for  $-d\epsilon/d\alpha$  behind the trapezoidal-wing tip of figure 4. For the region between the Mach cones from the tips of the leading and trailing edge of the wing (region 1),

$$-\frac{d\epsilon}{d\alpha} = \frac{1}{\pi} \left( -\log_e R + \tan^{-1} \frac{2R \cos \theta}{1-R^2} - \frac{\pi}{2} \right) \quad (1)$$

which, in the  $z = 0$  plane, reduces to

$$-\frac{d\epsilon}{d\alpha} = \frac{1}{\pi} \left( -\log_e |T| + 2 \tan^{-1} T - \frac{\pi}{2} \right) \quad (2)$$

For the region behind the Mach cone from the tip of the trailing edge of the wing (region 2),

$$-\frac{d\epsilon}{d\alpha} = \frac{1}{\pi} \left( -\log_e R + \log_e R' + \tan^{-1} \frac{2R \cos \theta}{1-R^2} - \tan^{-1} \frac{2R' \cos \theta'}{1-R'^2} \right) \quad (3)$$

which, in the  $z = 0$  plane, reduces to

$$-\frac{d\epsilon}{d\alpha} = \frac{1}{\pi} (-\log_e |T| + \log_e |T'| + 2 \tan^{-1} T - 2 \tan^{-1} T') \quad (4)$$

These equations are used to determine the theoretical value of  $-d\epsilon/d\alpha$  at each survey station.

The indications of linearized theory may be somewhat in error because of: (1) differences between the theoretical and the actual spanwise distributions of shed vorticity; (2) distortion and displacement of the vortex sheet; (3) volume distribution of vorticity; and (4) influence of the friction wake.

The qualitative influence of these modifying factors on the downwash in the vicinity of the vortex sheet will be discussed by considering the linearized solution for downwash in the Trefftz plane ( $x = \infty$ ) corresponding to each of these modifications. The reasons for using the Trefftz plane are: (1) The linearized solutions for downwash in this plane are easily obtained; and (2) the results obtained for the Trefftz plane give qualitative relations between the downwash and the shed vorticity that are applicable for analyzing the experimental data.

Spanwise distribution of shed vorticity. - According to linearized theory, the wing circulation  $\Gamma$  at a spanwise station is (reference 3)

$$\Gamma = \frac{U}{2} \int_{x_1}^{x_2} (C_{p,B} - C_{p,T}) dx \quad (5)$$

which becomes

$$\Gamma = -2\alpha U y_0 \quad (5a)$$

for the tip region ( $-c/\beta \leq y_0 \leq 0$ ) of the trapezoidal wing cut back along the inboard Mach line. Hence, the shed vorticity  $d\Gamma/dy_0$  is theoretically constant in this region. Viscous effects, however, may modify the theoretical spanwise distribution of circulation and, consequently, the spanwise distribution of shed vorticity at the trailing edge. In particular, flow separation upstream of the trailing edge would tend to reduce the wing circulation, with a proportionally greater reduction occurring at

the outboard tip where the chord is smallest. In addition, the vorticity in the trailing vortex system may redistribute itself as the fluid moves downstream.

In the Trefftz plane, the exact linearized value of  $-d\epsilon/d\alpha$  may be found from reference 3 as a function of  $d\Gamma/dy_0$  and equals

$$-\frac{d\epsilon}{d\alpha} = -\frac{1}{2\pi\alpha U} \int_{-\frac{c}{\beta}}^0 \frac{(y-y_0) \frac{d\Gamma}{dy_0}}{z^2 + (y-y_0)^2} dy_0 \quad (6)$$

The effect of the spanwise distribution of shed vorticity is shown in figure 5, where the values of  $-d\epsilon/d\alpha$  in the  $z = 0$  plane at infinity corresponding to constant, parabolic, and triangular distributions of  $d\Gamma/dy_0$  are compared for an assumed constant total strength of the shed vorticity. The parabolic and triangular distributions of vorticity represent possible modifications of the constant value predicted by linearized theory. The maximum value of  $-d\epsilon/d\alpha$  is seen to shift closer to the center of the theoretical vortex sheet when the vorticity changes from constant to triangular distribution. The downwash at points outboard of the wing tip is less sensitive to variations in the distribution of shed vorticity but does depend on changes in the total strength of the shed vorticity. The distribution of wing circulation that produces each distribution of vorticity is also shown in figure 5. The constant, parabolic, and triangular distributions of shed vorticity progressively concentrate more and more vorticity in the center of the theoretical shed-vortex sheet. The limiting case is then a single line vortex along the line  $\beta y/c = -0.5$ . The downwash corresponding to this line vortex is also included in figure 5.

Distortion and displacement of vortex sheet. - Linearized theory assumes the shed-vortex sheet to be in the  $z = 0$  plane. In practice, the vortex sheet is distorted and displaced from the  $z = 0$  position. Changes in the configuration and orientation of the vortex sheet constitute vortex-sheet distortion in this report. Vortex-sheet displacement is considered to be the average displacement of the individual streamlines of the trailing vortex system. The qualitative effect of this distortion and displacement will be determined by considering the Trefftz plane behind the trapezoidal wing.

1. Distortion. The downwash in the  $z = 0$  plane is symmetrical about  $\beta y/c = -0.5$  and thus tends to rotate the vortex sheet about this station as an axis. The effect of such a rotation on the downwash distribution in the  $z = 0$  plane is shown in figure 6 for several slopes  $m$  of the vortex sheet with respect to the  $y$ -axis. The maximum value of  $-d\epsilon/dx$  is seen to decrease in magnitude and to shift closer to  $\beta y/c$  as  $m$  is increased.

2. Displacement. The vortex sheet may be displaced as a unit from the  $z = 0$  plane. The effect of the vortex-sheet displacement is indicated in figure 7. The downwash in the  $z = 0$  plane is plotted for different displacements  $\beta z/c$  of the vortex sheet. As the distance between the  $z = 0$  plane and the plane containing the vortex sheet is increased, the magnitude of  $-d\epsilon/dx$  in the  $z = 0$  plane decreases.

Volume distribution of vorticity. - Linearized theory indicates that the trailing vorticity behind the wing tip is in the form of a vortex sheet. The vorticity is actually distributed, however, throughout a finite volume. The effect of the volume distribution is shown in figure 8 where the theoretical shed vorticity for the trapezoidal wing is assumed to be distributed uniformly throughout a volume of thickness  $t$ . The thickness effect modifies the singularity in downwash, predicted by linearized theory, at the edges of the vortex sheet but is negligible otherwise.

Influence of friction wake. - It has been found (reference 4) that the friction wake behind an airfoil at subsonic speeds induces a flow of air towards the wake center. The inflow of air increases the downwash above the wake and decreases the downwash below the wake. The magnitude of this effect is small, except for wings with high-drag flaps or for partly stalled wings. The influence of the friction wake on the downwash behind a supersonic wing has not yet been determined.

## RESULTS AND DISCUSSION

Experimental and theoretical variations of downwash angles with angle of attack are compared in figures 9 and 10. The theoretical values are obtained from equations (2) and (4). The agreement between linearized theory and experiment at each survey station depends on the location of that station with respect to the shed-vortex sheet. This agreement and the relative influence of the modifying factors mentioned in the theory will be discussed.

## Downwash at Spanwise Stations

Downwash angle as a function of angle of attack for spanwise stations a and b is presented in figure 9(a) and 9(b), respectively. For stations within about two chord lengths behind the leading edge of the wing, the curves are linear and the slopes are generally in reasonably good agreement with theory. As previously noted, the downwash at points well outboard of the wing tip depends mainly on the total strength of the shed vorticity and is relatively insensitive to variations in the distribution of the shed vorticity. Thus, the agreement in this region indicates that the total strength of the shed vorticity is approximately that assumed in linearized theory. The slight differences between theory and experiment are attributed to experimental error. The discontinuities in the curves for points 15a and 19a may be caused by shock waves from the wing or their reflection from the tunnel walls (fig. 4). Curves for points 15b and 19b fall below the theoretical values at the higher angles of attack, which may be caused by distortion and displacement of the vortex sheet.

Station c and d lie near the edge of the vortex sheet; data plotted for each point in these stations (figs. 9(c) and 9(d)) indicate that  $-d\epsilon/d\alpha$  decreases continuously with increasing positive angle of attack. This effect could be caused by modifications of the spanwise distribution of shed vorticity, such as those shown in figure 5, and by an increasing distortion and displacement of the shed-vortex sheet with angle of attack. For points 3 to 6, distortion and the displacement of the vortex sheet is relatively small and the decreasing slope is probably caused primarily by differences between the theoretical and the actual distribution of shed vorticity. At stations 11, 15, and 19, the deviation from theory is greater. Inasmuch as the distortion and the displacement of the vortex sheet is greater for these stations, this factor also contributes to the deviation from theory in this region.

At stations e, f, and g, the magnitude of  $-d\epsilon/d\alpha$  generally increases with positive angle of attack (figs. 9(e) to 9(g)), which is opposite to the trend observed at stations c and d. The greatest deviation from theory occurs at station e. Modifications of the spanwise distribution of shed vorticity and the distortion of the vortex sheet (as shown in figs. 5 and 6) are the most important factors causing this deviation. Small modifications of the distribution of shed vorticity or the distortion of the vortex sheet could account for the high value of  $-d\epsilon/d\alpha$  at  $0^\circ$  angle of attack noted at station e. The reversed slope noted at low angles of attack for stations 3e and 4e may be caused by a strong upflow at the trailing edge of the wing.

At station h (fig. 9(h)), the magnitude of  $-d\epsilon/d\alpha$  is lower at higher positive angles of attack than at  $0^\circ$  angle of attack. Inasmuch as station h lies near the edge of the vortex sheet, the effect of distortion and displacement of the vortex sheet and the assumed modified distribution of vorticity are theoretically similar to their effects at stations c and d. Comparison of figure 9(h) with figures 9(c) and 9(d) shows that in each case the slope of the downwash curve decreases as the angle of attack is increased, so that the expected correspondence in variation of downwash with angle of attack appears to be confirmed. The influence of outflow or inflow near the viscous wake, which should be largest at station h, appears to be relatively unimportant because no effects are observed in figure 9(h) that can be specifically attributed to the viscous wake. Thus, no definite conclusions regarding the wake effect are possible. The discontinuities in the value of  $-d\epsilon/d\alpha$  for point 7h may be caused by shock waves from the trailing edge of the wing.

#### Downwash at Chordwise Stations

The theoretical and experimental curves for the spanwise variation of  $-d\epsilon/d\alpha$  at each chordwise station are presented in figure 10. The slopes of the experimental curves of downwash angle as a function of angle of attack (fig. 9) were measured for each station at angles of attack of  $0^\circ$  and  $7^\circ$ . Curves were faired through the experimental points in figure 10 to show significant trends. The curves are not definitely established by the small number of experimental points in sections near the maximum values of  $-d\epsilon/d\alpha$ . A series of short dashes indicate the uncertain fairing in these sections for an angle of attack of  $7^\circ$ . For an angle of attack of  $0^\circ$ , the experimental points do not preclude the possibility of very large values near  $\beta y/c = 0, -1$ ; thus no fairing was made near these points.

In general, the theoretical and experimental curves follow the same trends at an angle of attack of  $0^\circ$ . At an angle of attack of  $7^\circ$ , however, the spanwise location of the maximum value of  $-d\epsilon/d\alpha$  occurs at a point nearer the center of the theoretical vortex sheet ( $\beta y/c = -0.5$ ). This trend indicates that the principal factors that modify the linearized downwash solution for the trapezoidal-wing tip are modifications of the spanwise distribution of shed vorticity and the distortion of the vortex sheet. (Compare fig. 10 with figs. 5 and 6.)

## Wake Survey

Results of the wake survey are plotted in figure 11 as  $\Delta H/H$  against  $\beta z/c$  for stations e and g at an angle of attack of  $0^\circ$ . The intensity of the wake is defined by

$$\frac{\Delta H}{H} = \frac{H - H_w}{H}$$

The free-stream pitot pressure was calculated from the free-stream total pressure and Mach number. The pitot pressures in the wake were measured directly. As would be expected, the intensity of the wake diminished as the distance behind the trailing edge increased.

The displacement of the maximum wake intensity at stations e and g is plotted as a function of  $x/c$  in figure 12. For comparison, theoretical curves for wake displacement obtained from the equation (reference 5)

$$z = (z)_t - \int_{x_t}^x \tan \epsilon \, dx \quad (7)$$

are also plotted in figure 12 for  $4^\circ$  angle of attack. Theoretical values of  $\epsilon$  based on equations (2) and (4) were used in the computation of these curves.

At station e, the wake displacement decreases in the downwash region just behind the wing and increases in the upwash region farther behind the wing for positive angles of attack. At station g, the wake displacement decreases steadily for positive angles of attack because downwash is found throughout this station. Thus it is seen that the wake displacement at these stations follows the trends indicated by linearized theory. The differences between experimental and theoretical wake displacement may be explained in part by the fact that the wake center may lie somewhat above the trailing edge because of flow separation on the top surface of the wing. Thus, the experimental curve is displaced in the positive direction from the theoretical curve for each station. Inasmuch as the wake should follow the streamlines, the small differences between the local slopes of the theoretical and experimental curves are probably caused by the fact that the actual values of  $\epsilon$  at the wake differ from the theoretical values used in equation (7).

## SUMMARY OF RESULTS

An experimental investigation has been conducted at a Mach number of 1.91 to determine the downwash in the region of the trailing vortex system behind a trapezoidal-wing tip.

For small angles of attack, the experimental spanwise variation of  $-d\epsilon/d\alpha$  (where  $\epsilon$  is the downwash angle and  $\alpha$  is the angle of attack) at each chordwise station was generally similar to the variation predicted by linearized theory. At higher angles of attack, the maximum value of  $-d\epsilon/d\alpha$  occurred nearer the center of the theoretical vortex sheet than linearized theory would indicate. This result was attributed to differences between the theoretical and actual spanwise distribution of vorticity, and the distortion of the vortex sheet, but the individual effects generally could not be isolated.

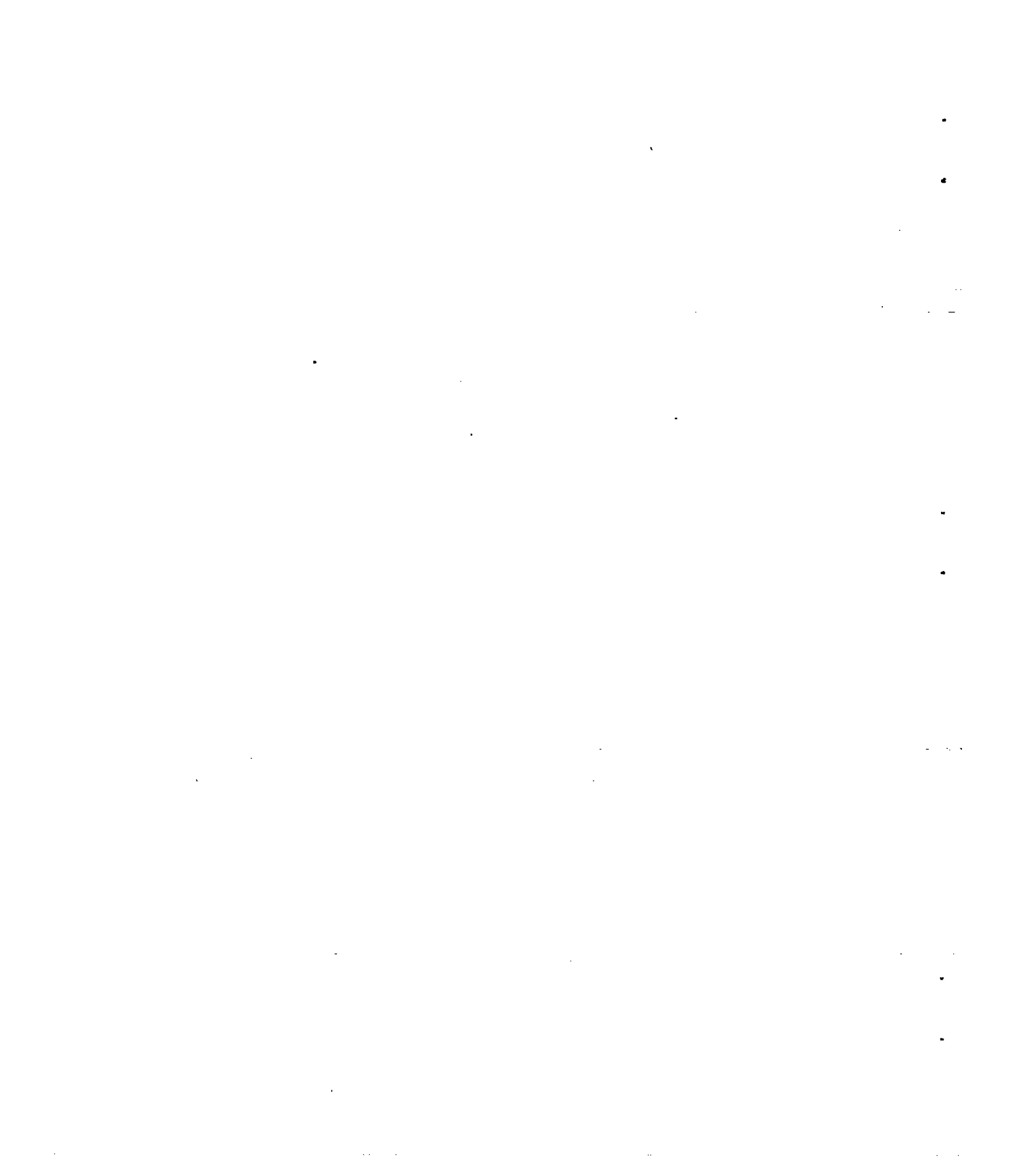
As in subsonic flow, the wake profile expanded and lost intensity at points farther behind the wing. At the trailing edge of the wing, the wake center appeared to lie somewhat above the wing. This effect was attributed to flow separation ahead of the trailing edge.

Lewis Flight Propulsion Laboratory,  
National Advisory Committee for Aeronautics,  
Cleveland, Ohio.

## REFERENCES

1. Lagerstrom, P. A., and Graham, Martha: Downwash and Sidewash Induced by Three-Dimensional Lifting Wings in Supersonic Flow. Rep. No. SM-13007, Douglas Aircraft Co., Inc., April 14, 1947.
2. Heaslet, Max A., and Lomax, Harvard: The Calculation of Downwash behind Supersonic Wings with an Application to Triangular Plan Forms. NACA TN 1620, 1948.
3. Mirels, Harold, and Haefeli, Rudolph C.: Line-Vortex Theory for Calculation of Supersonic Downwash. NACA TN 1925, 1949.
4. Silverstein, Abe, Katzoff, S., and Bullivant, W. Kenneth: Downwash and Wake behind Plain and Flapped Airfoils. NACA Rep. 651, 1939.

5. Perkins, Edward W., and Canning, Thomas N.: Investigation of Downwash and Wake Characteristics at a Mach Number of 1.53. I - Rectangular Wing. NACA RM A8L16, 1949.



0811

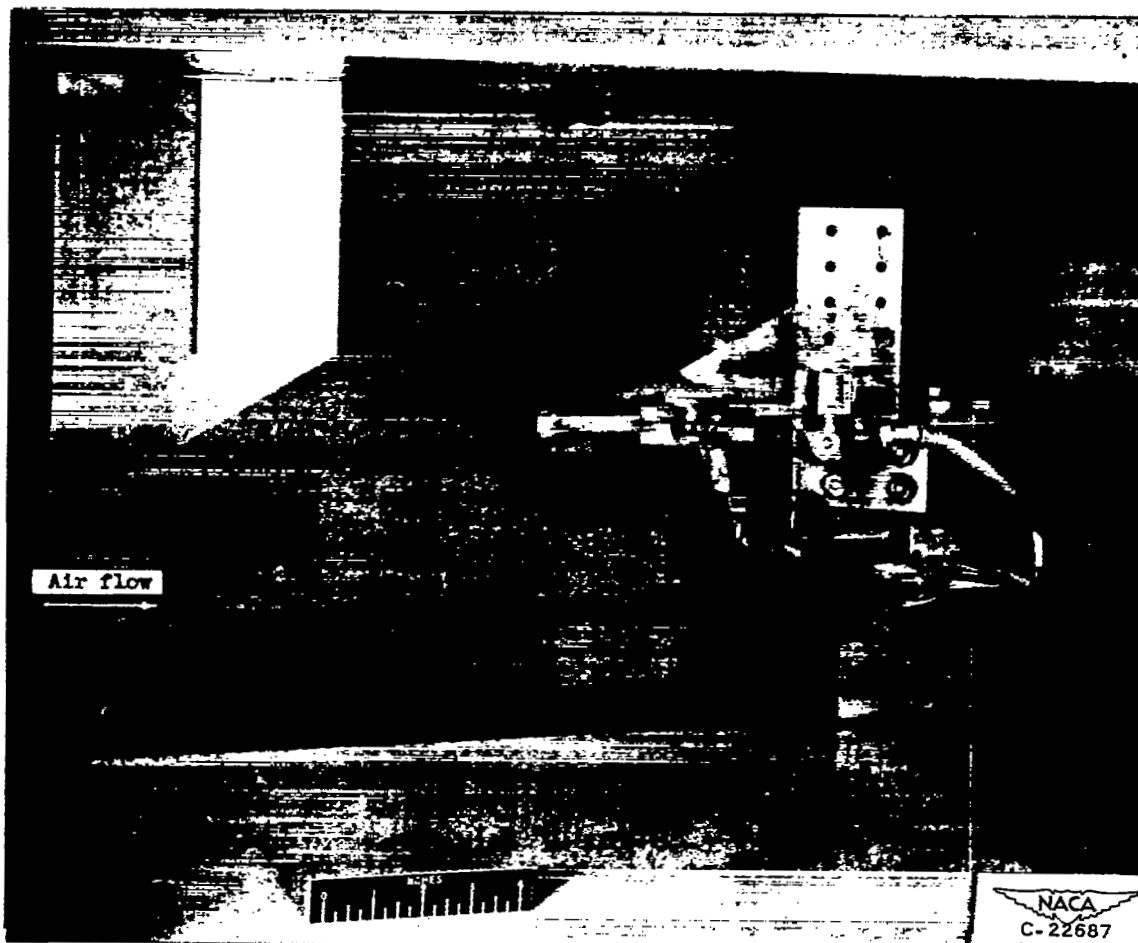
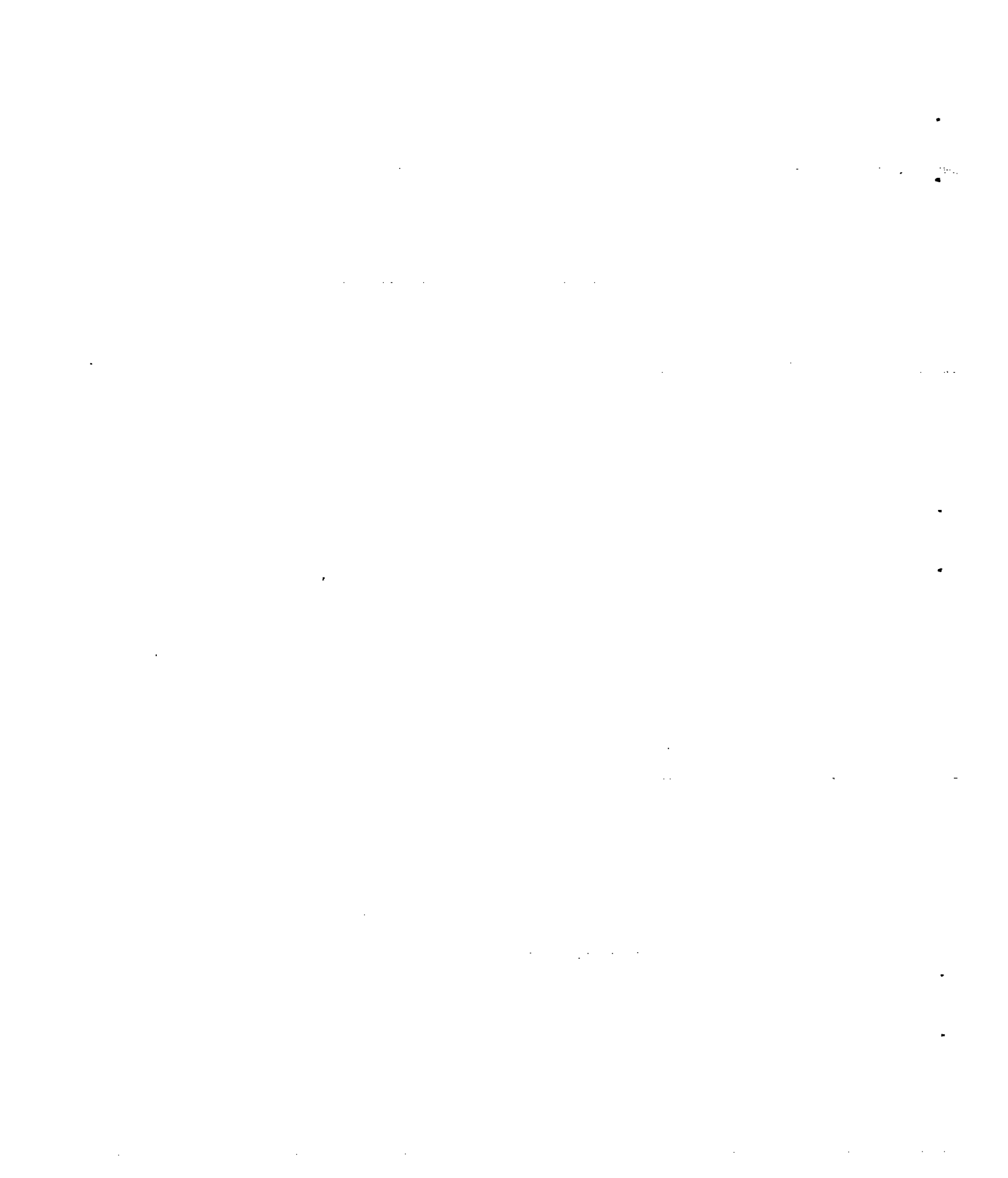


Figure 1. - Test section with wing and downwash mechanism installed.



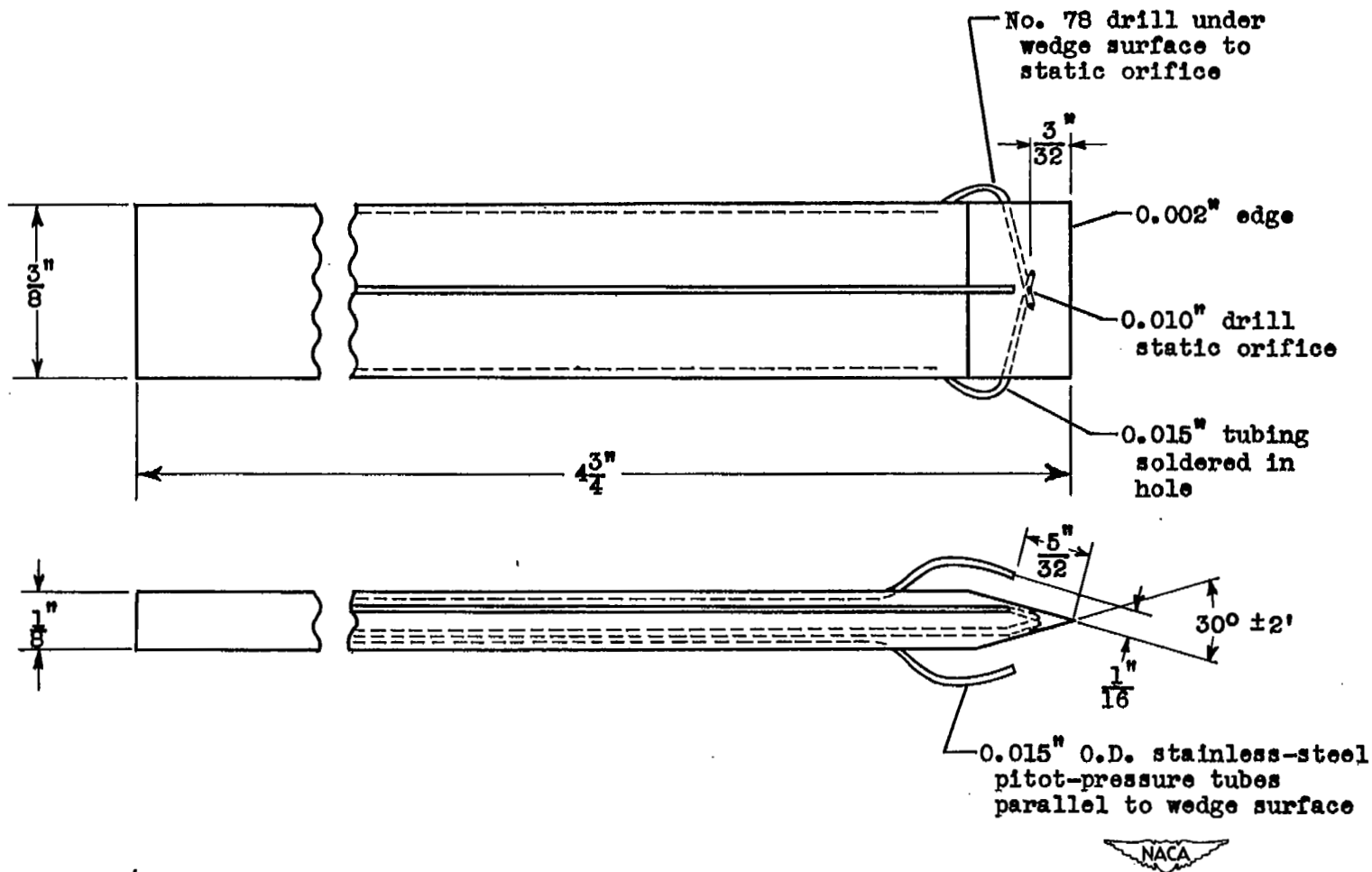


Figure 2. - Wedge used for measuring downwash.



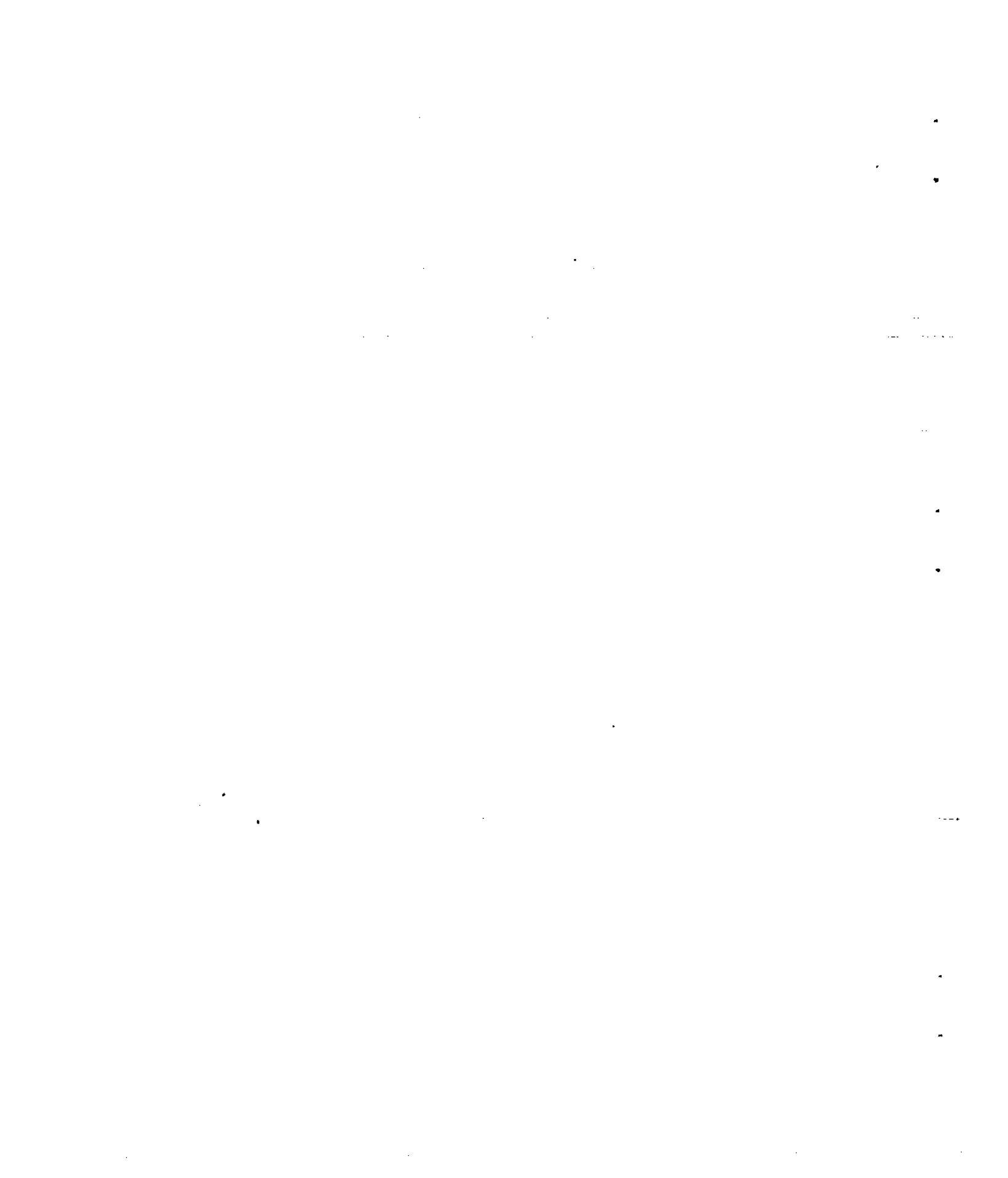
1180



(a) Details of rake.



(b) Rake installed in tunnel.  
Figure 3. - Pitot-pressure rake.



0811

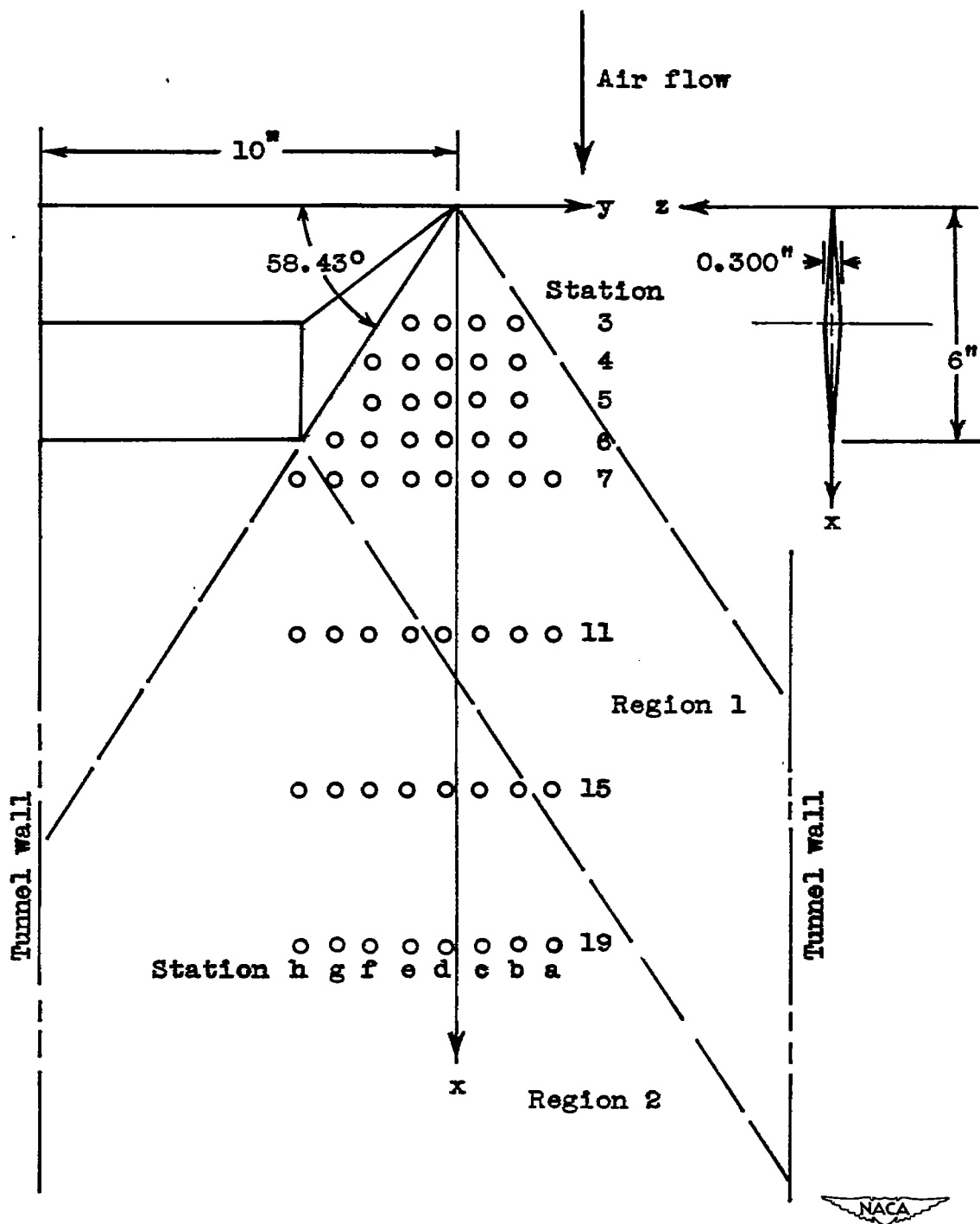


Figure 4. - Trapezoidal wing and survey stations.

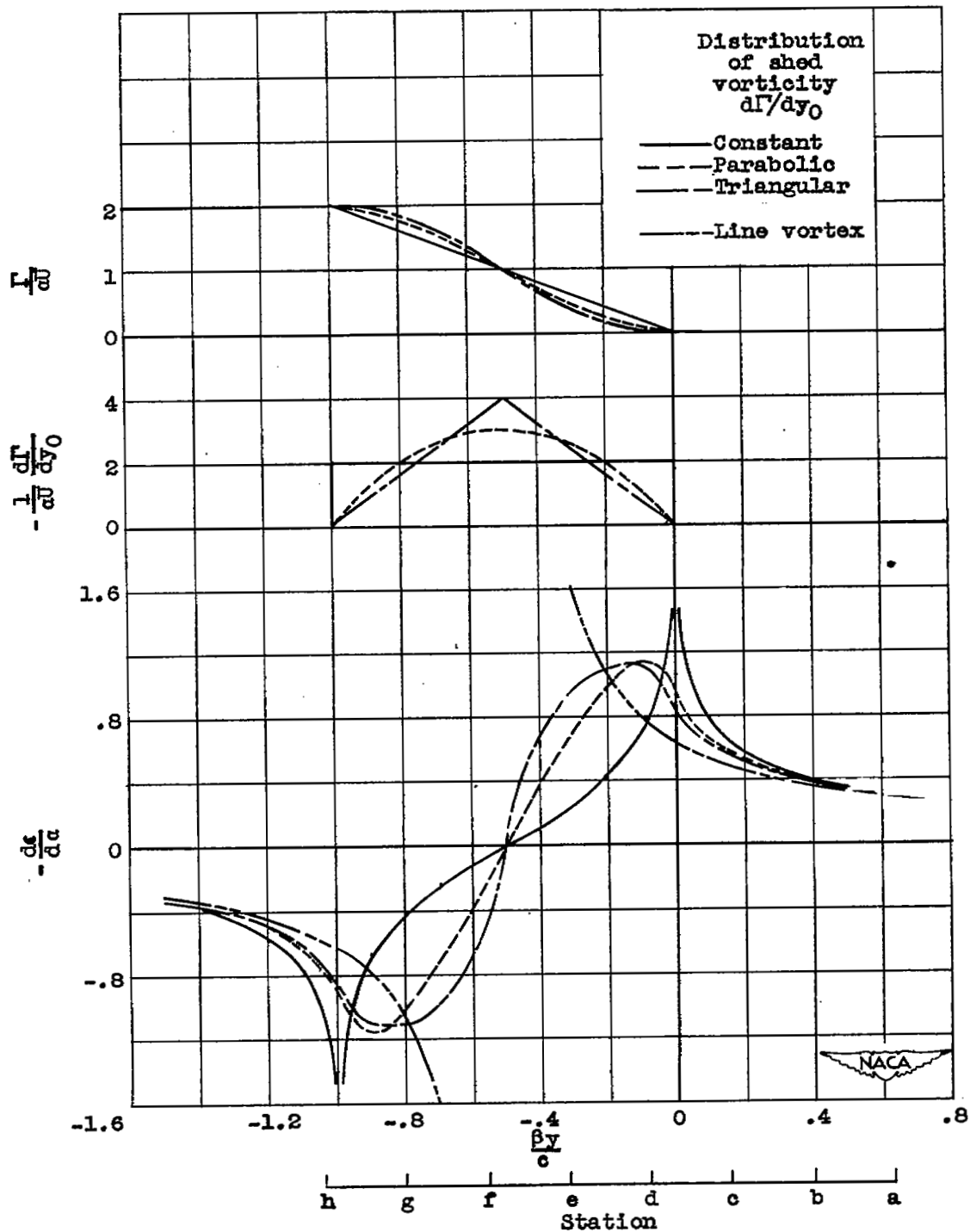


Figure 5. - Several spanwise distributions of shed vorticity  $d\Gamma/dy_0$ , corresponding circulation distributions  $\Gamma$ , and corresponding distributions of  $-dc/da$  at  $x = \infty$ ,  $z = 0$ .

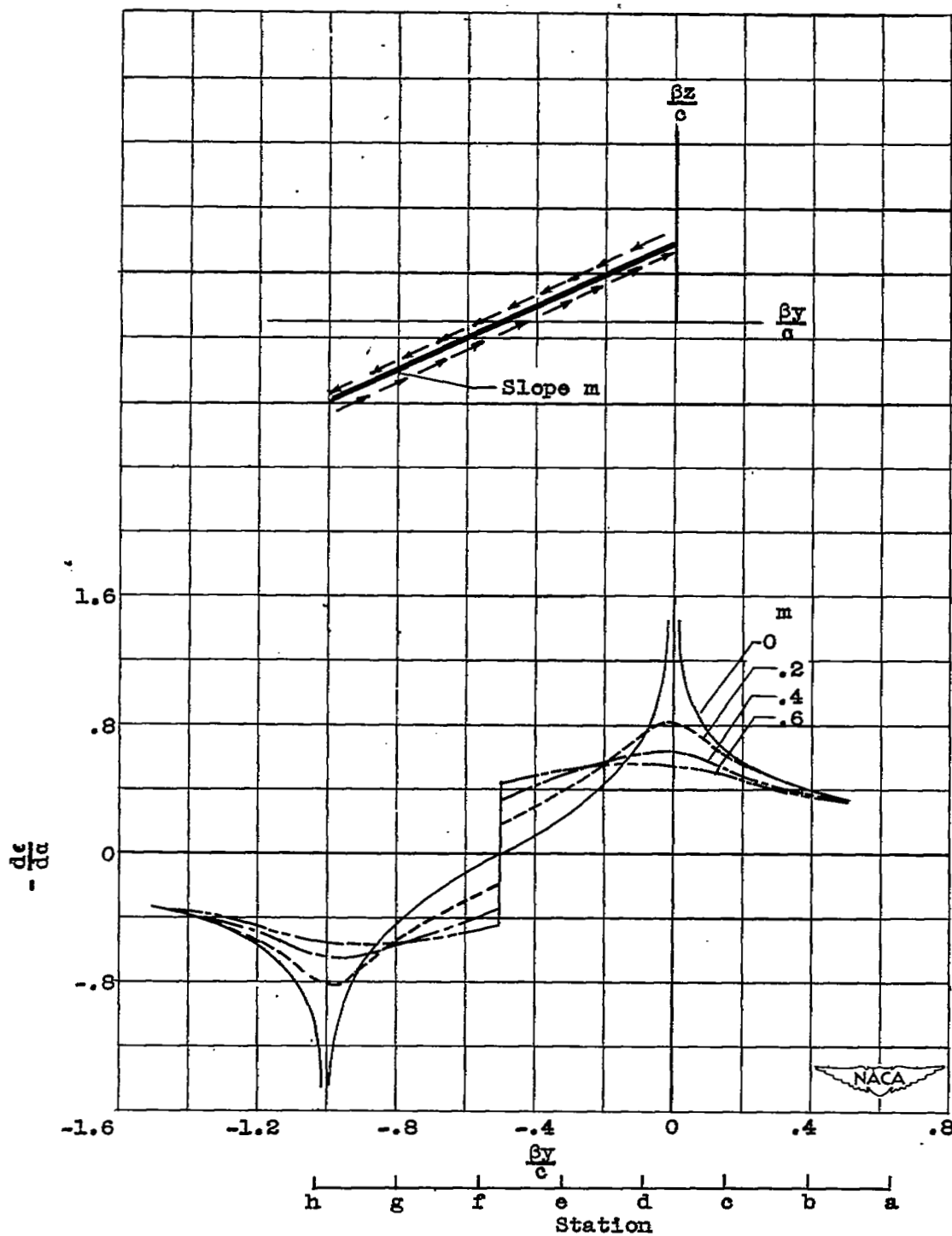


Figure 6. - Spanwise distribution of  $-\frac{dc}{da}$  at  $x = \infty$ ,  $z = 0$  for vortex sheet rotated about  $\beta y/c = -0.5$ .

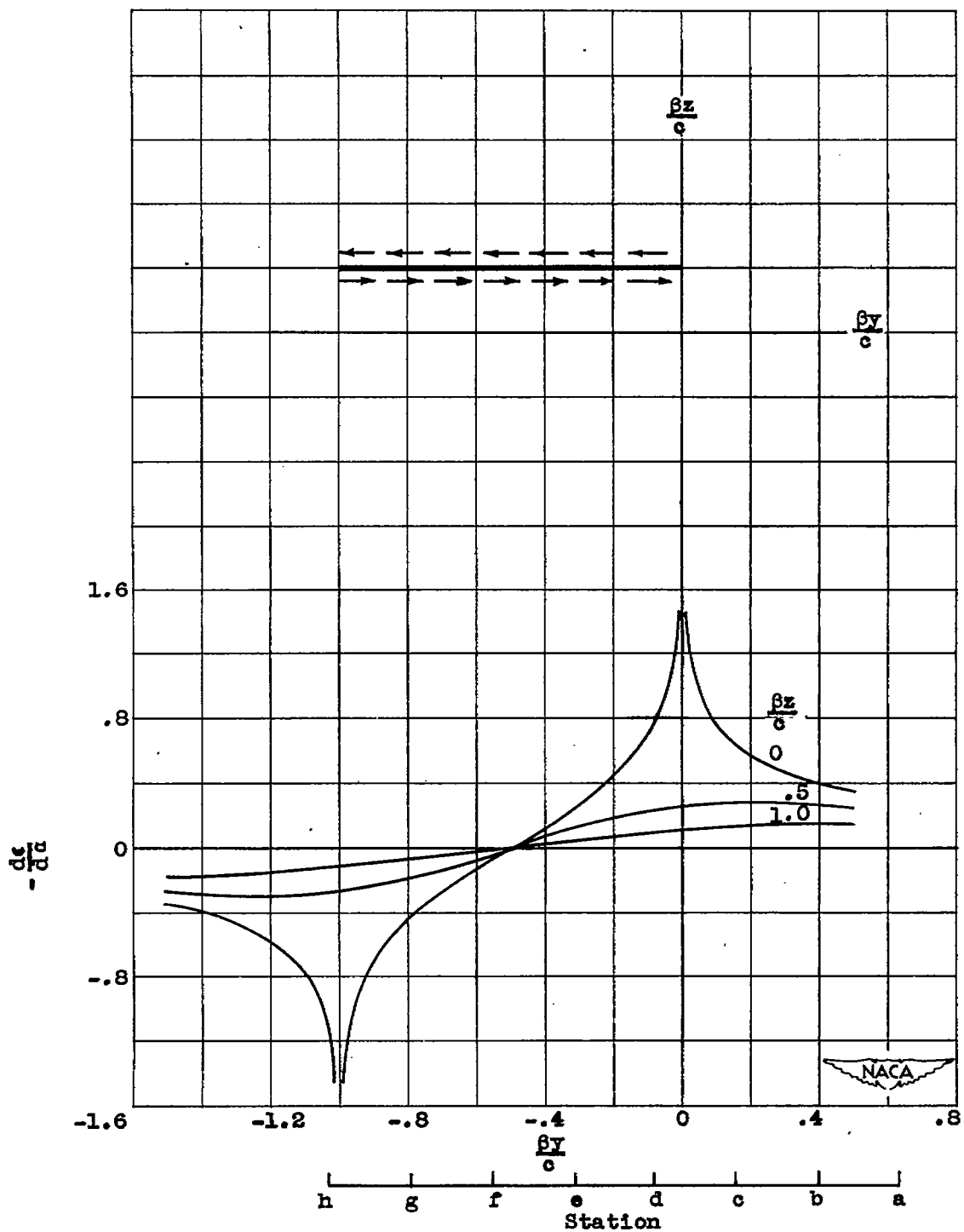


Figure 7. - Spanwise distribution of  $-\frac{d\epsilon}{dc}$  at  $x = \infty$  with vortex-sheet displacement.

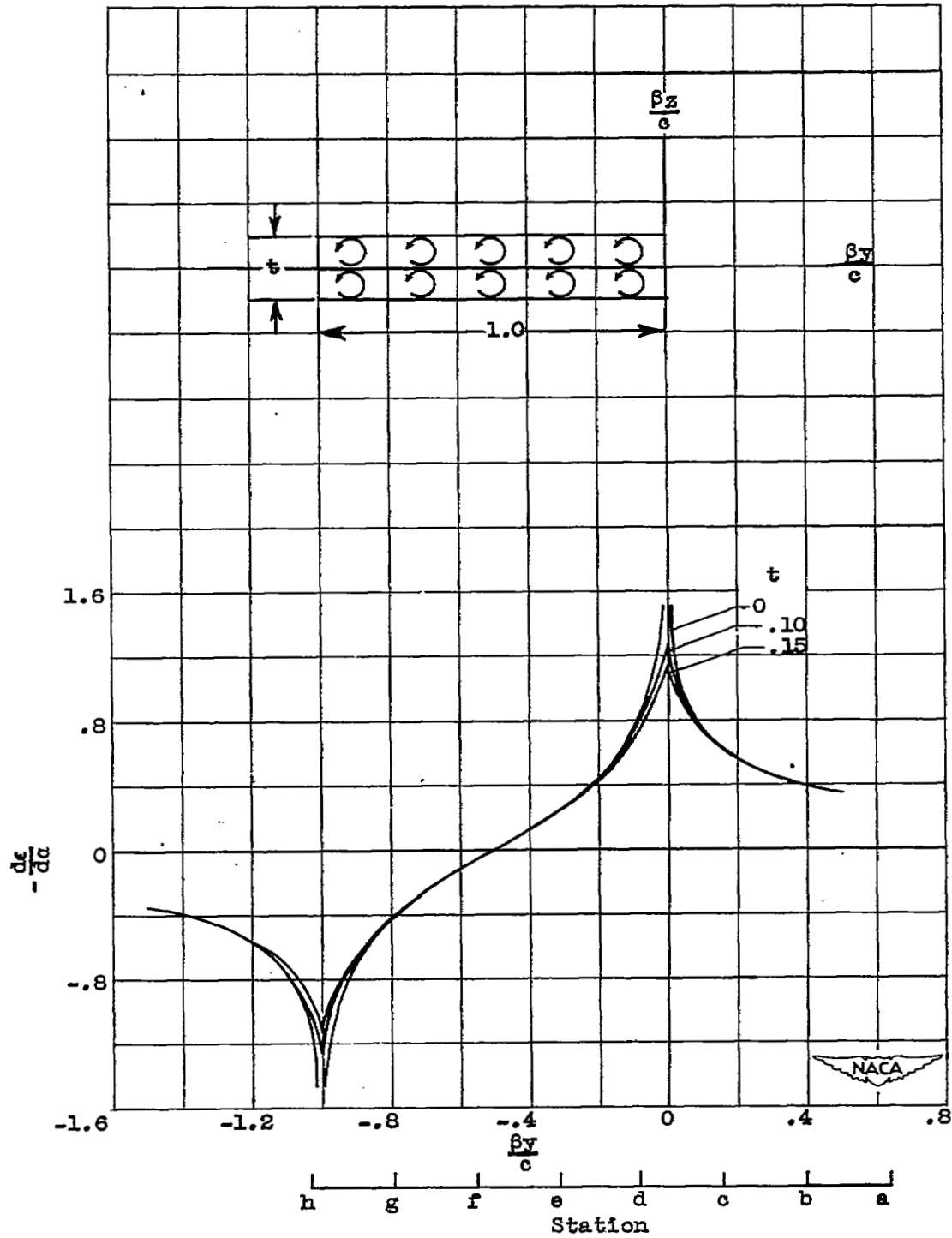


Figure 8. - Spanwise distribution of  $-\frac{d\epsilon}{d\alpha}$  at  $x = \infty$ ,  $z = 0$  with volume distributions of vorticity.

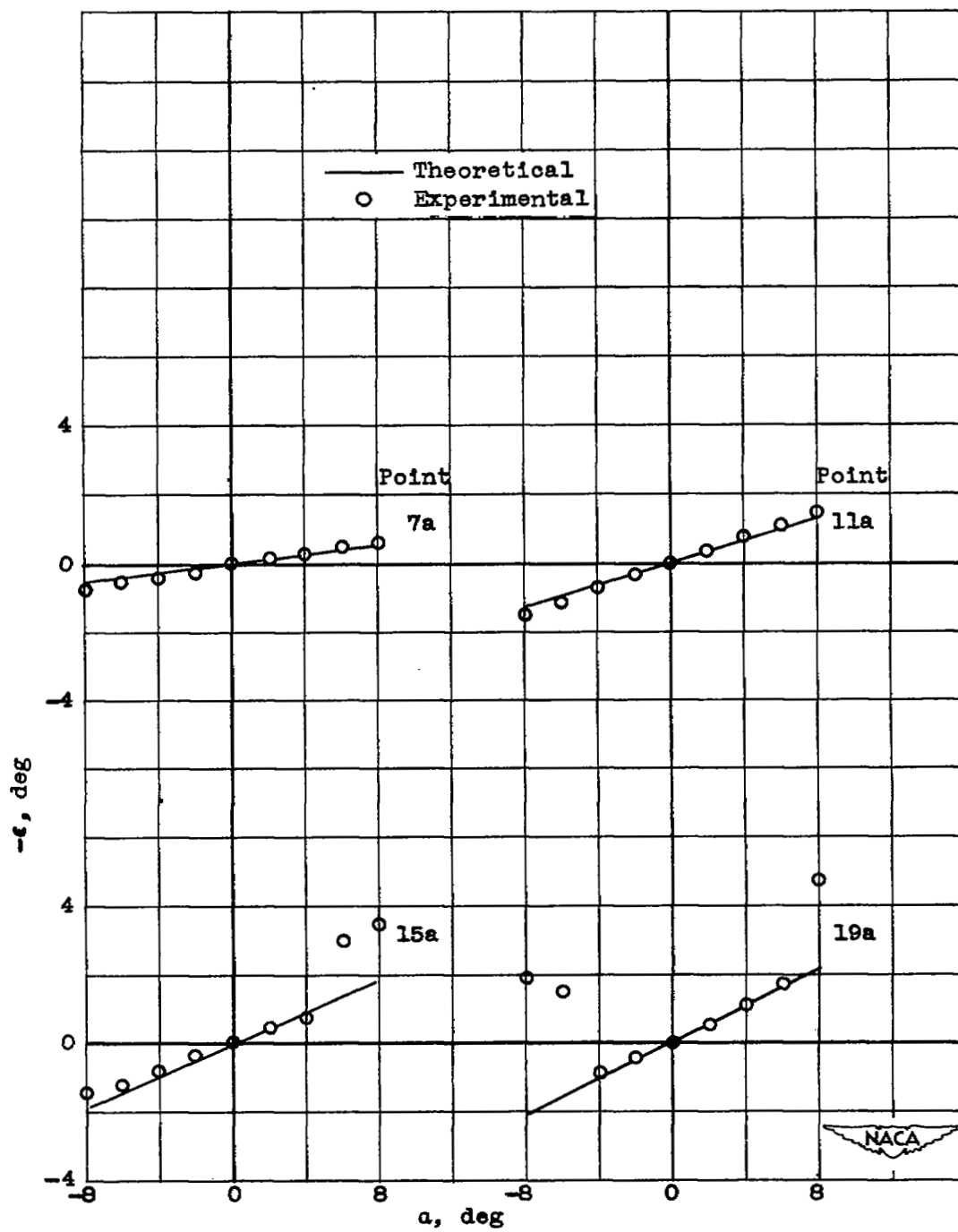
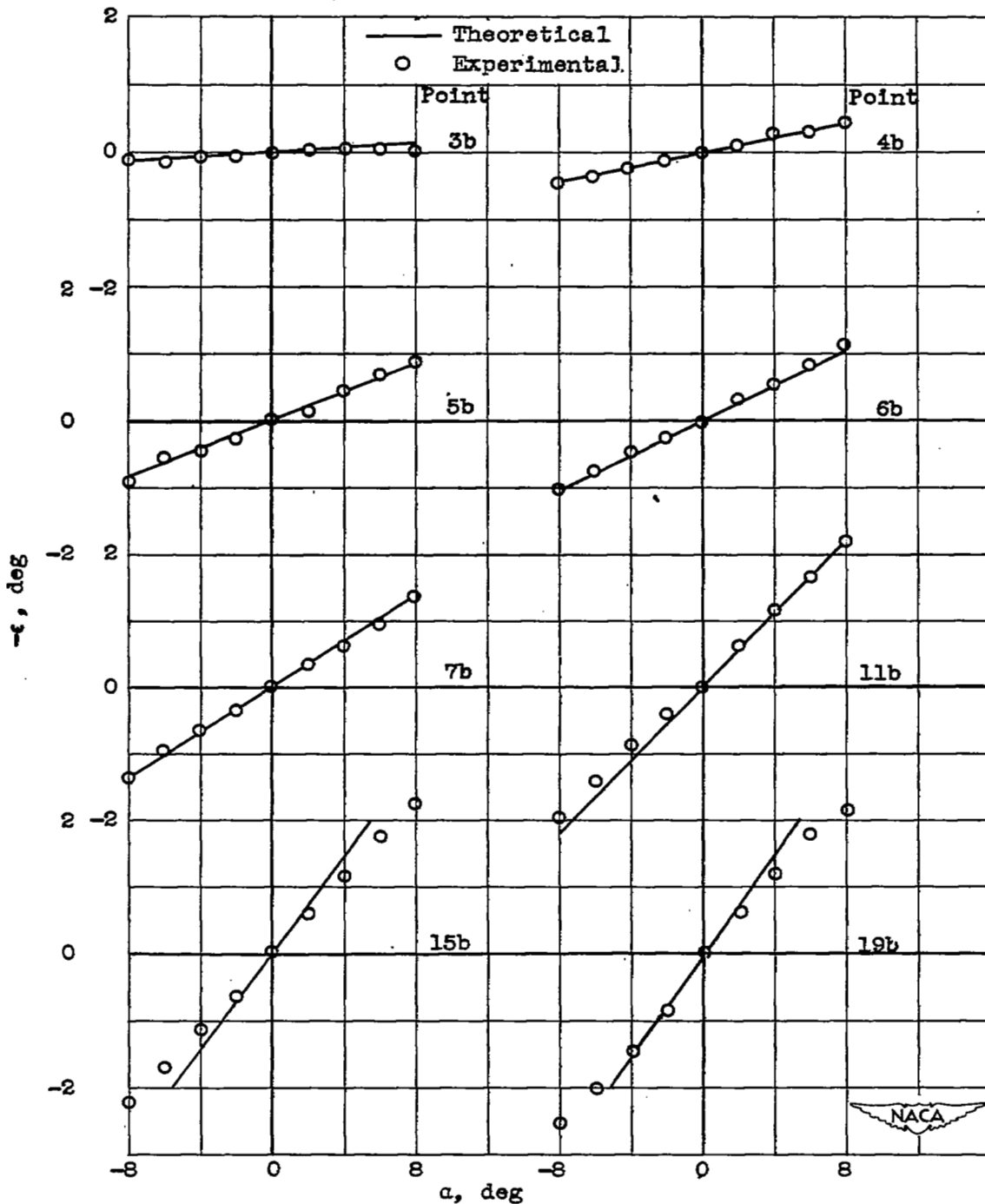
(a) Station a;  $\beta y/c = 0.6305$ .

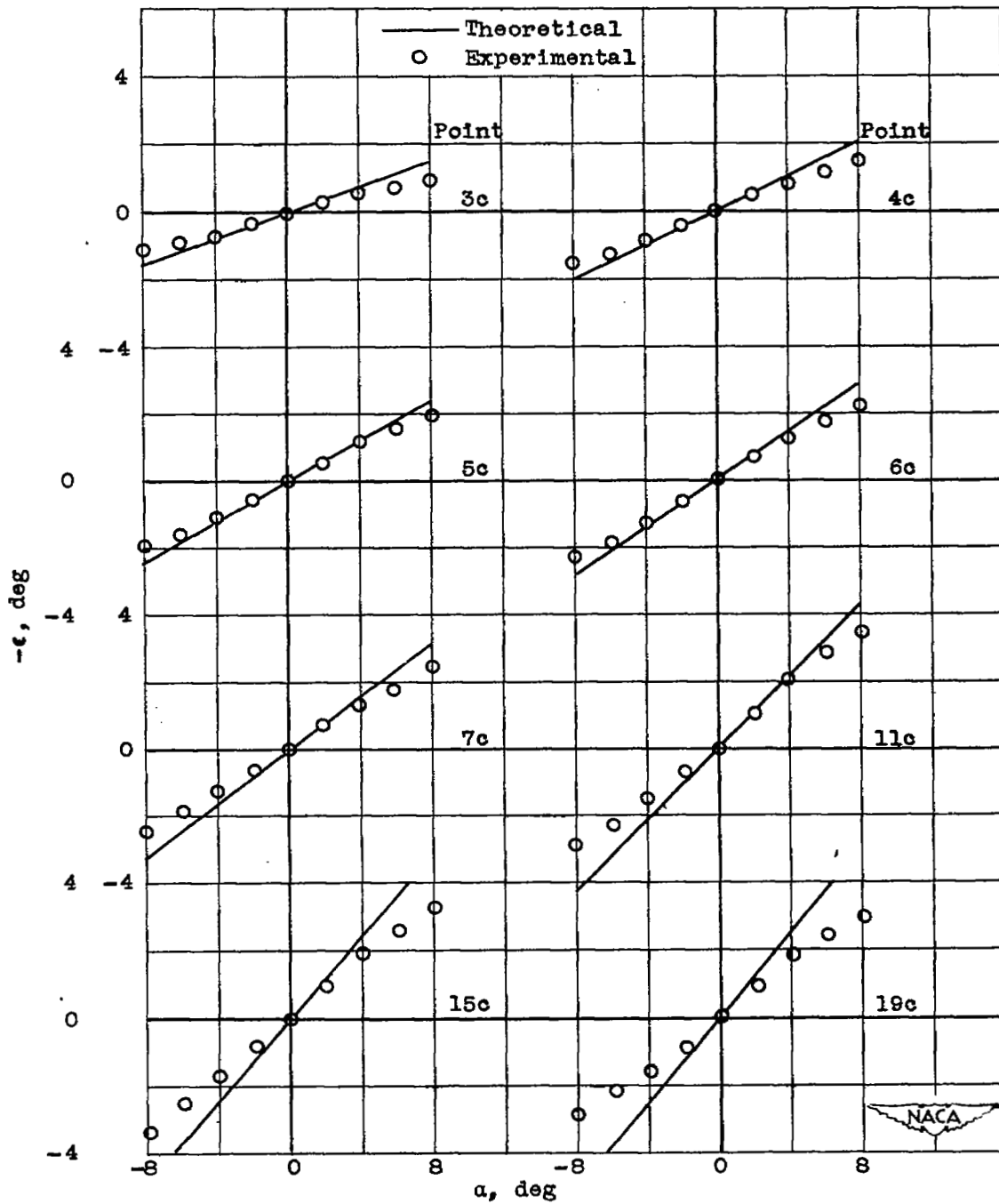
Figure 9. - Variation of downwash angle with angle of attack at spanwise station.

1180



(b) Station b;  $\beta y/c = 0.3935$ .

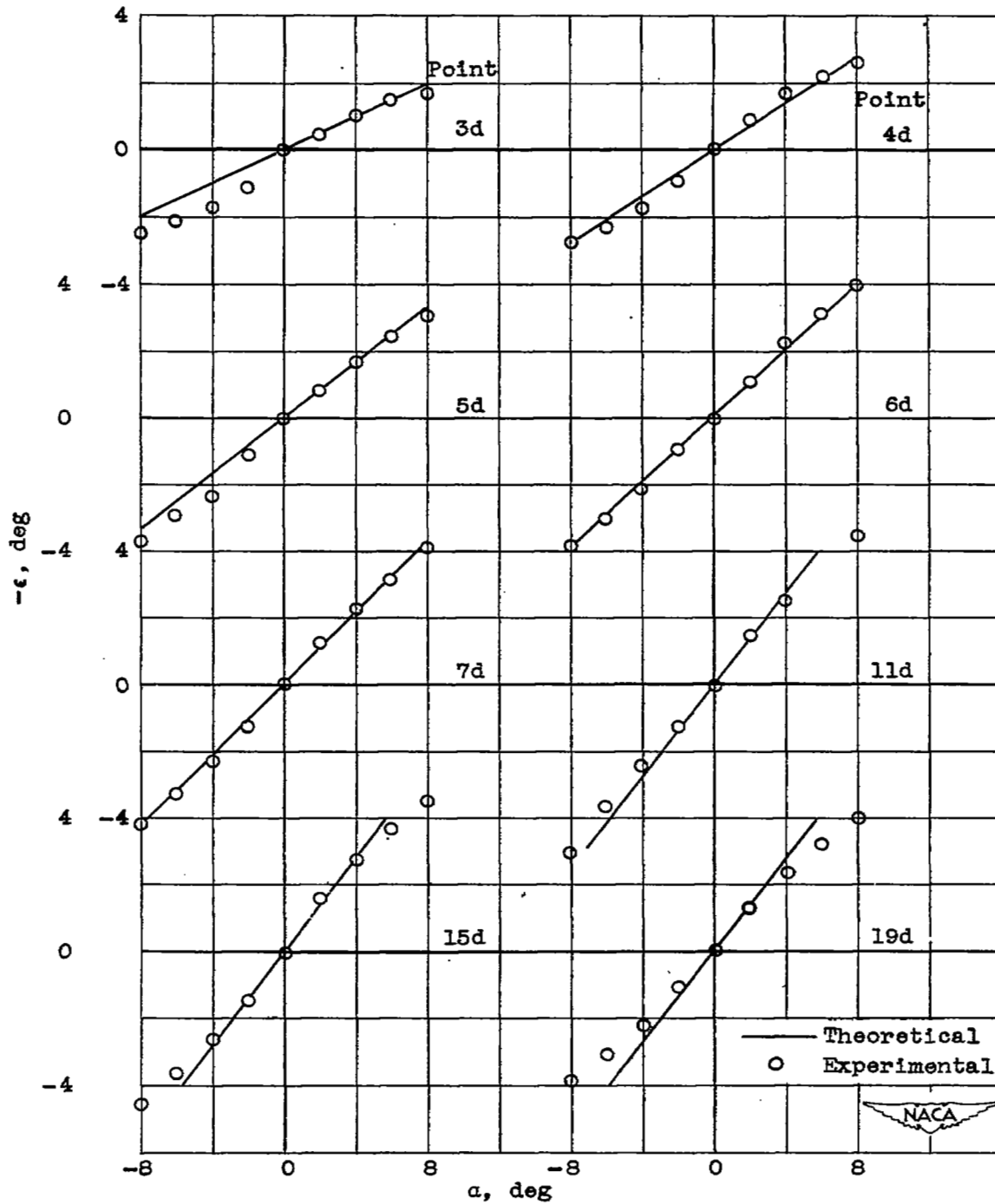
Figure 9. - Continued. Variation of downwash angle with angle of attack at spanwise station.



(c) Station  $c$ ;  $\beta y/c = 0.1560$ .

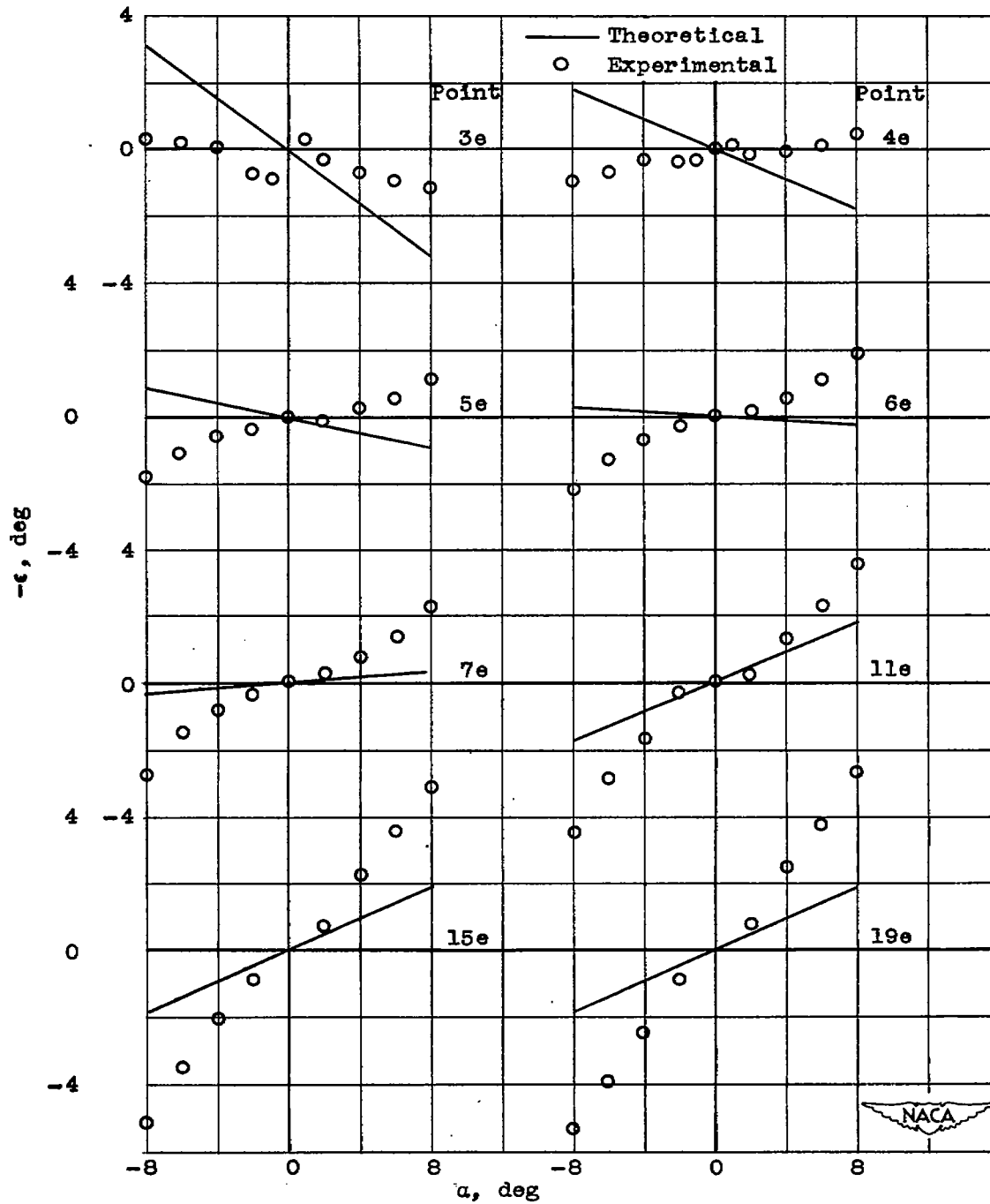
Figure 9. - Continued. Variation of downwash angle with angle of attack at spanwise station.

1180



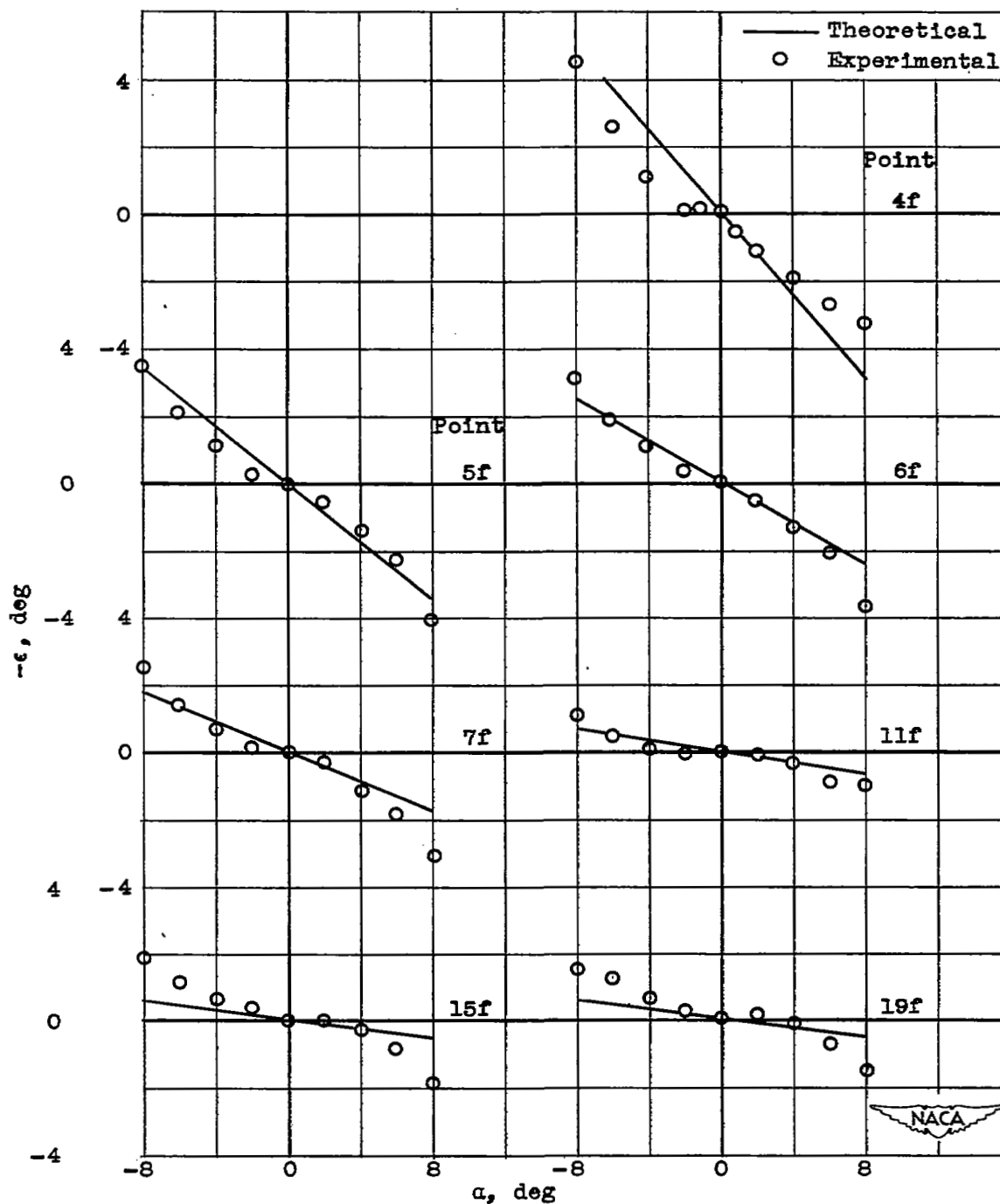
(d) Station d;  $\beta y/c = -0.0814$ .

Figure 9. - Continued. Variation of downwash angle with angle of attack at spanwise station.



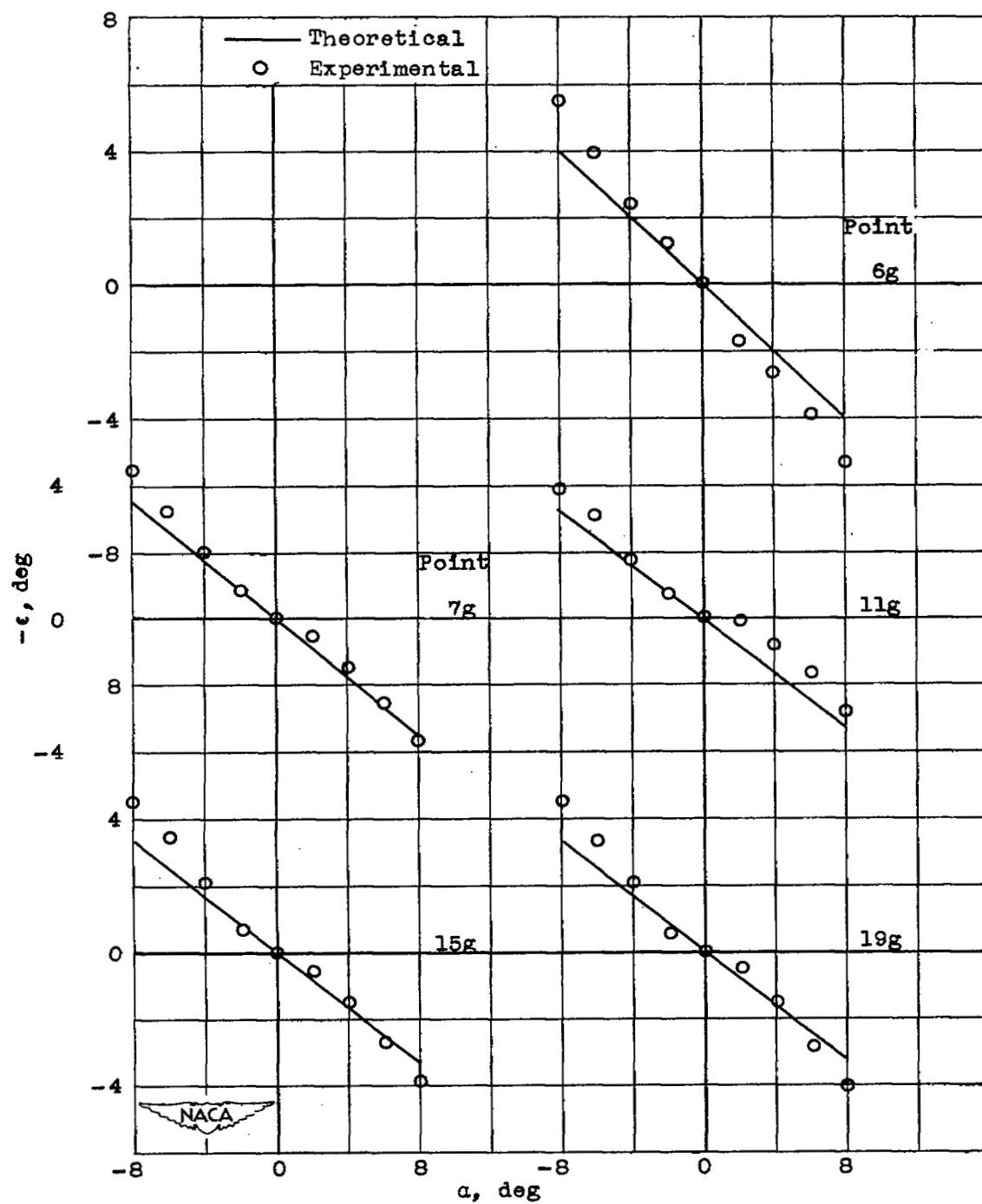
(e) Station e;  $\beta y/c = -0.3190$ .

Figure 9. - Continued. Variation of downwash angle with angle of attack at spanwise station.



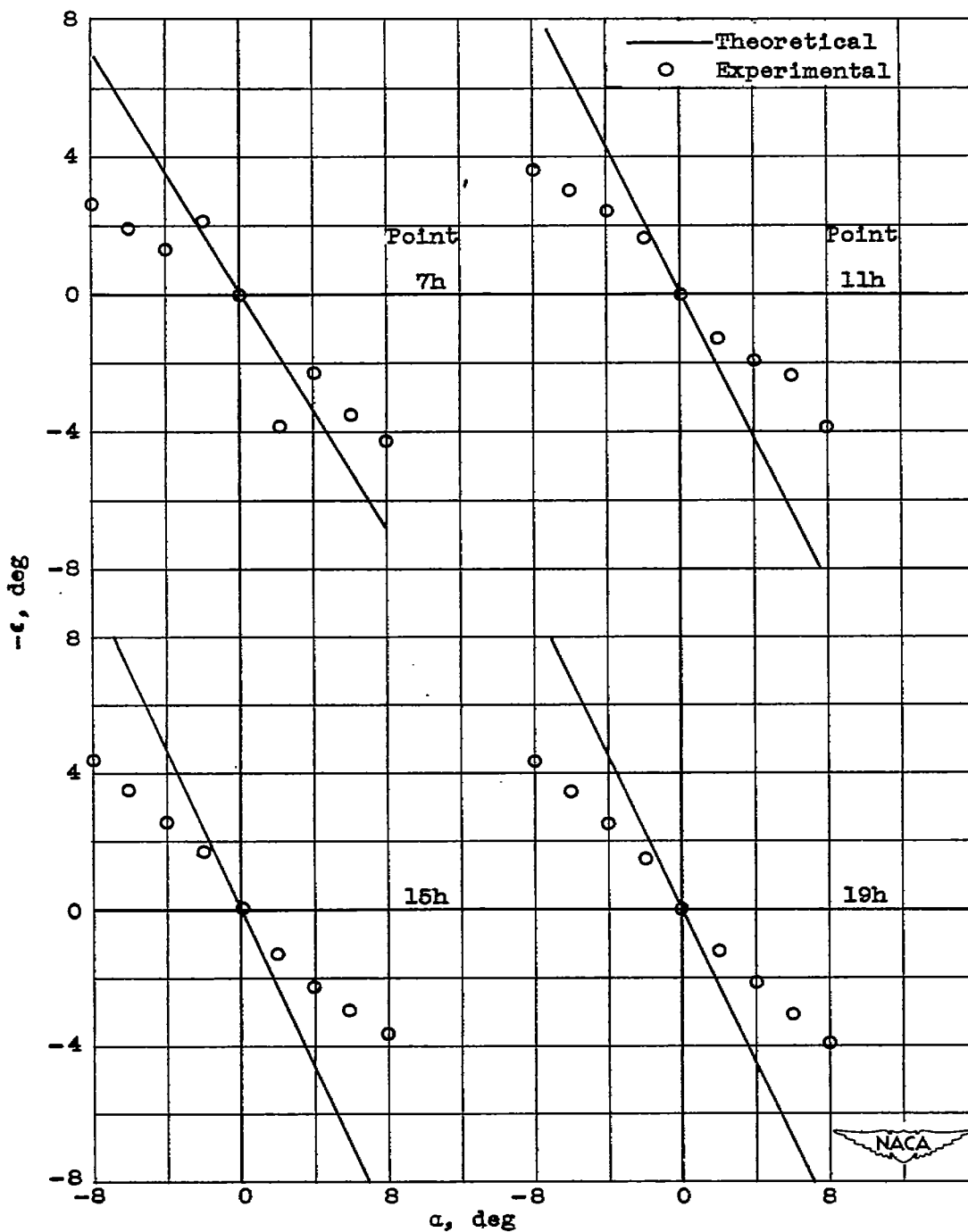
(f) Station f;  $\beta y/c = -0.5560$ .

Figure 9. - Continued. Variation of downwash angle with angle of attack at spanwise station.



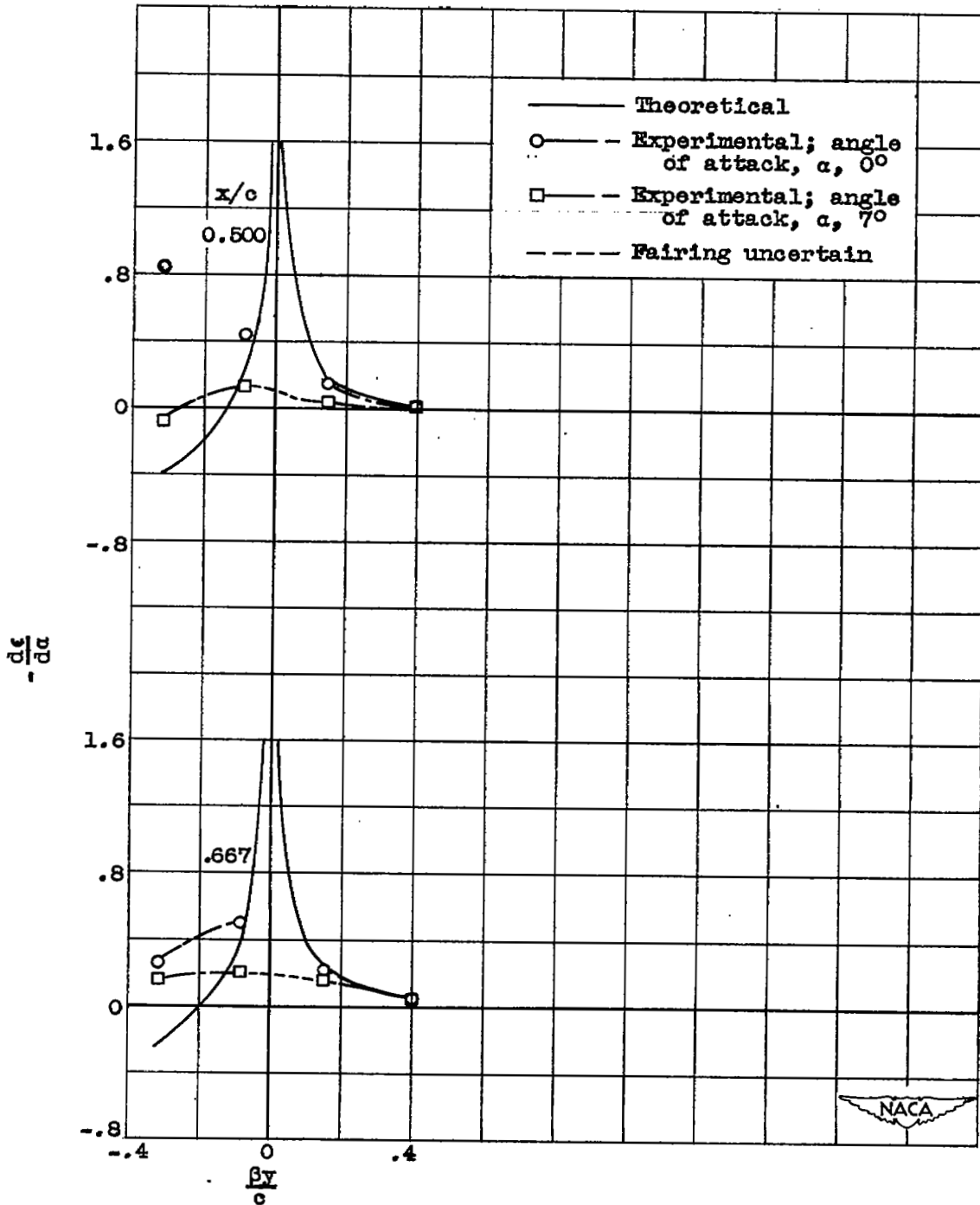
(g) Station g;  $\beta y/c = -0.7930$ .

Figure 9. - Continued. Variation of downwash angle with angle of attack at spanwise station.



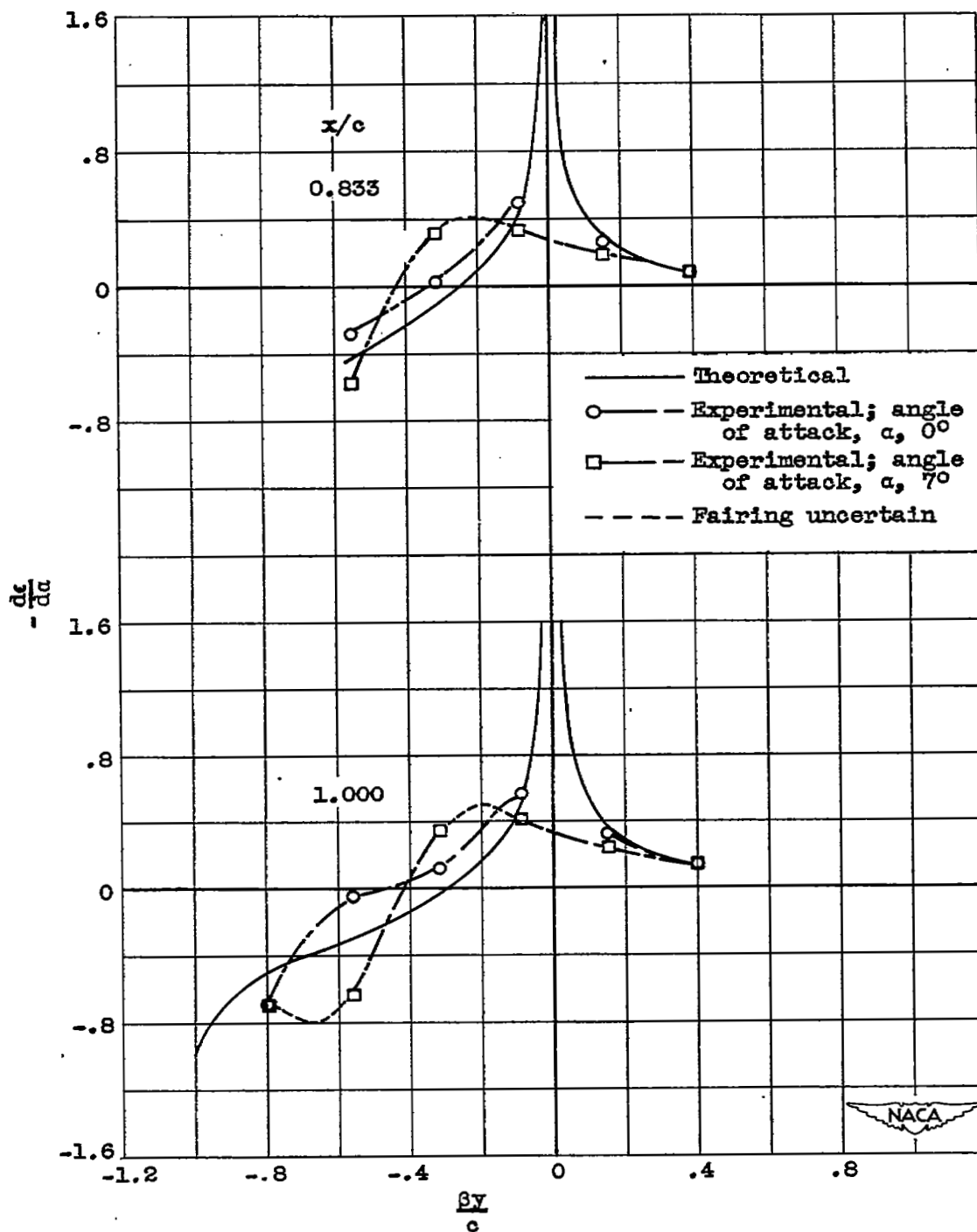
(h) Station h;  $\beta y/c = -1.031$ .

Figure 9. - Concluded. Variation of downwash angle with angle of attack at spanwise station.



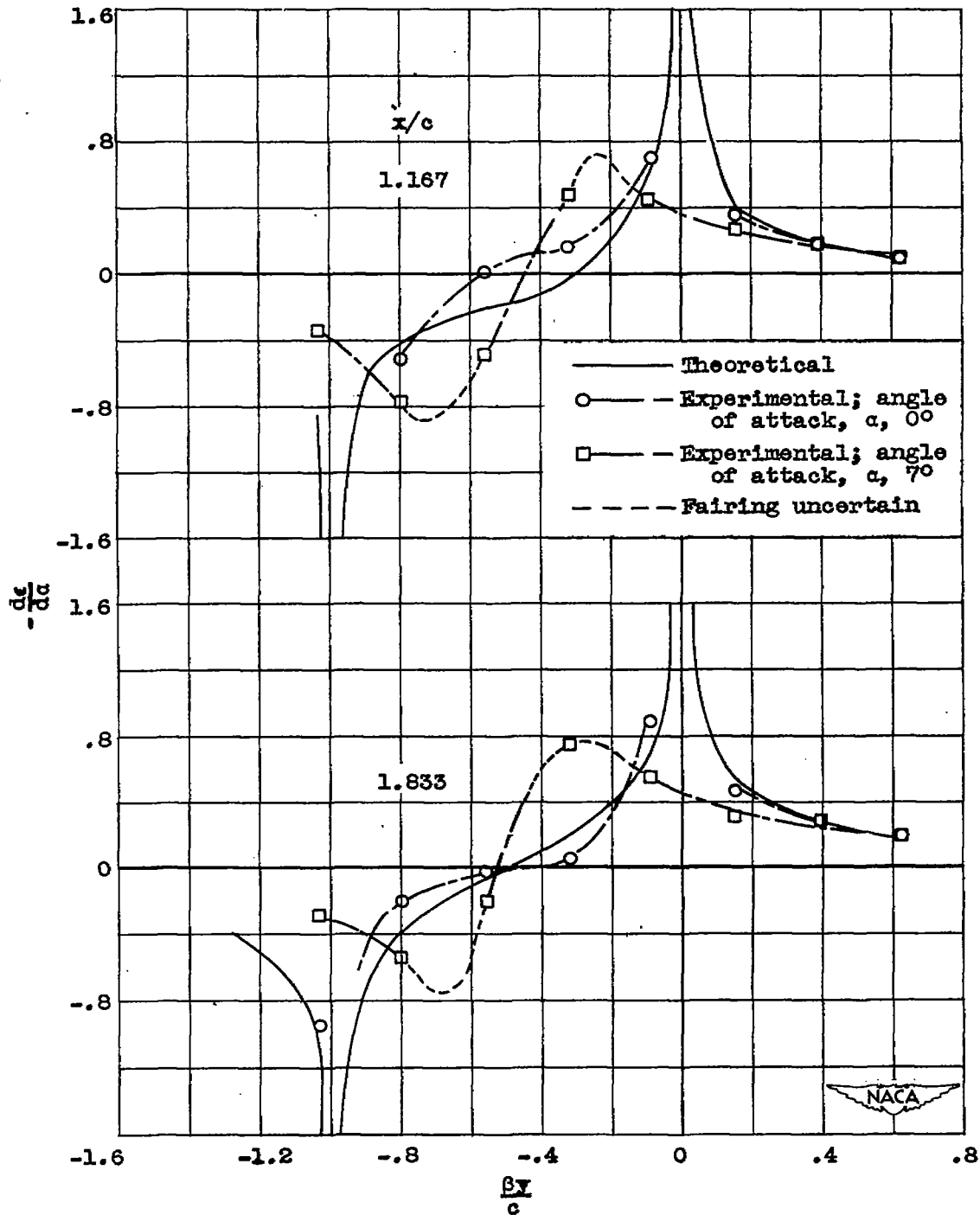
(a) Stations 3 and 4.

Figure 10. - Variation of  $-\frac{d\epsilon}{d\alpha}$  with  $\frac{\beta y}{c}$  for chordwise stations.



(b) Stations 5 and 6.

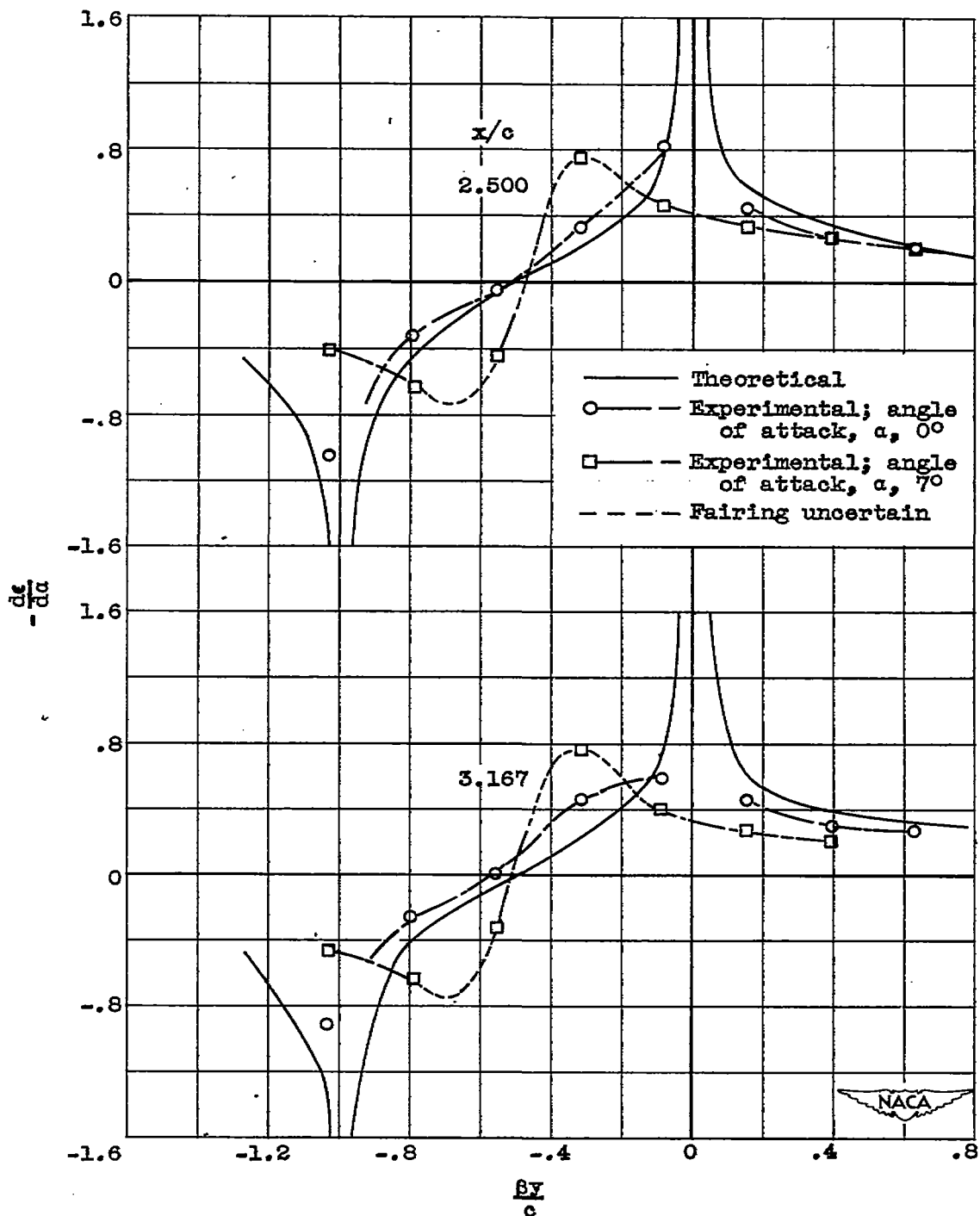
Figure 10. - Continued. Variation of  $-\frac{dc}{d\alpha}$  with  $\beta y/c$  for chord-wise stations.



(c) Stations 7 and 11.

Figure 10. - Continued. Variation of  $-d\epsilon/d\alpha$  with  $\beta y/c$  for chord-wise stations.

1180



(d) Stations 15 and 19.

Figure 10. - Concluded. Variation of  $-\frac{d\delta}{d\alpha}$  with  $\beta y/c$  for chordwise stations.

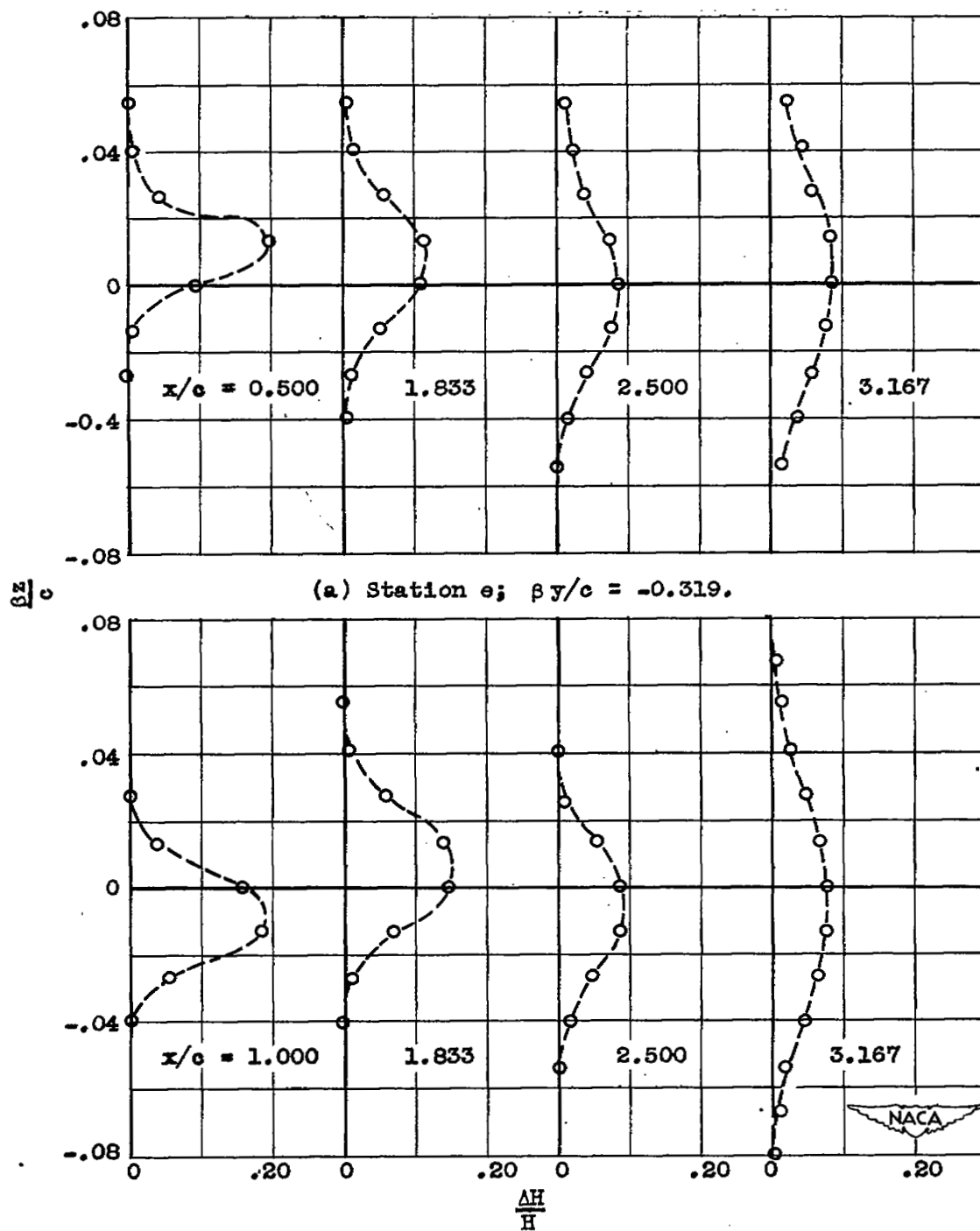
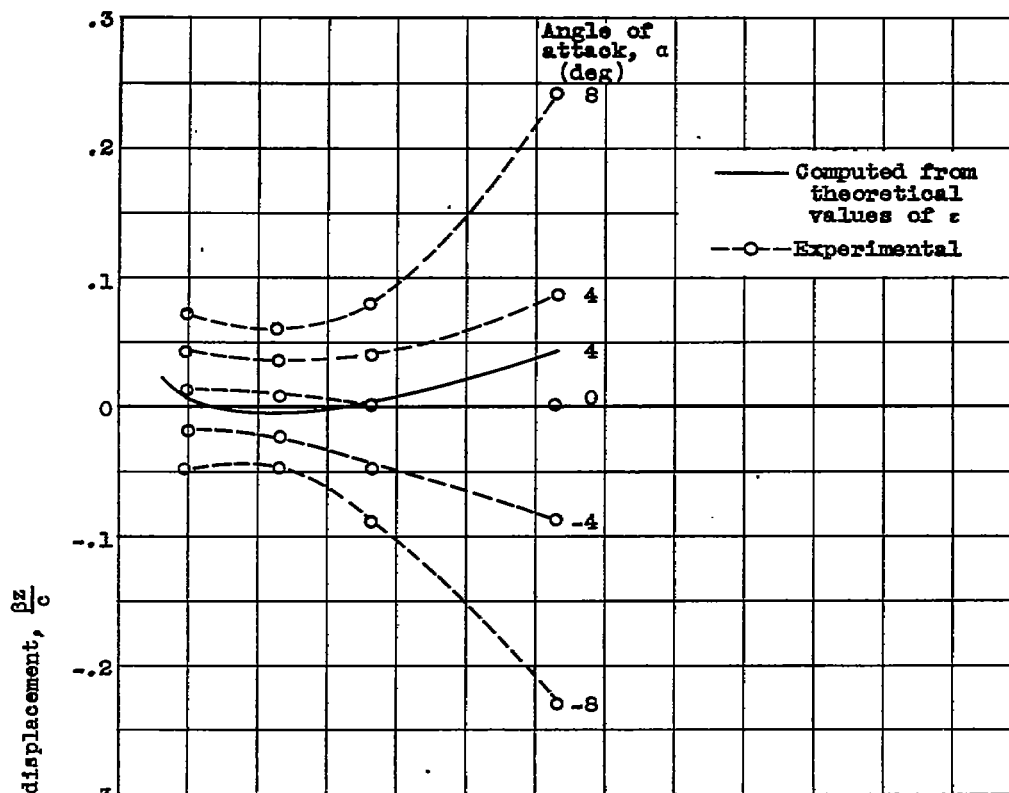
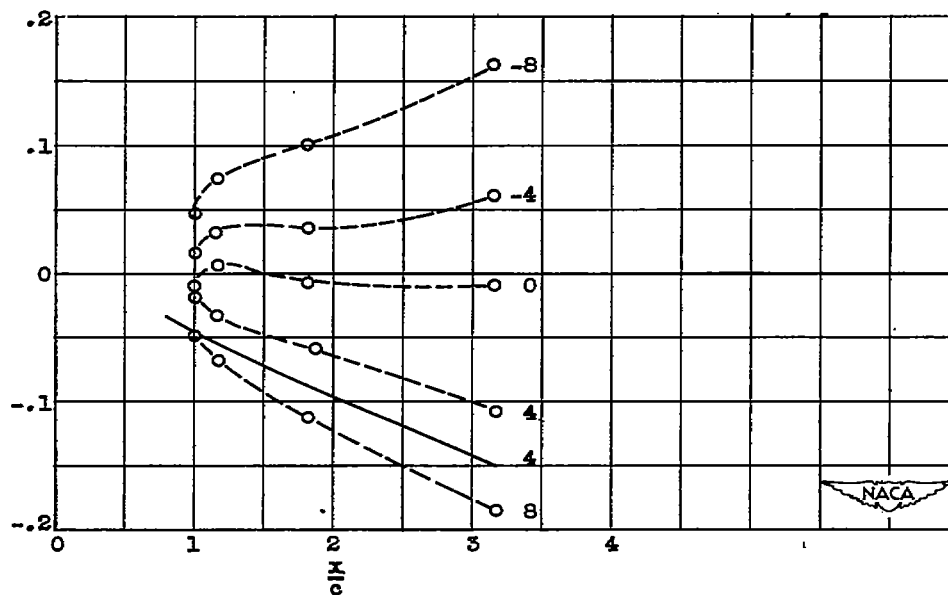


Figure 11. - Profiles of  $\Delta H/H$  through viscous wake of trapezoidal wing for stations e and g. Angle of attack,  $\alpha$ ,  $0^\circ$ .



(a) Station e;  $\beta y/c = -0.319$ .



(b) Station g;  $\beta y/c = -0.793$ .

Figure 12. - Chordwise variation of wake displacement.

NASA Technical Library



3 1176 01434 9238